

PAPER








Cite this: *Green Chem.*, 2020, **22**, 6084

Received 1st July 2020,
Accepted 2nd September 2020

DOI: 10.1039/d0gc02236e

rsc.li/greenchem

In situ electro-synthesis of anthraquinone electrolytes in aqueous flow batteries†

Yan Jing,  ‡^a Min Wu,  ‡^b Andrew A. Wong,  ^b Eric M. Fell,  ^b Shijian Jin,  ^b Daniel A. Pollack,  ^c Emily F. Kerr, ^a Roy G. Gordon  *^{a,b} and Michael J. Aziz  *^b

We demonstrate the electrochemical oxidation of an anthracene derivative to a redox-active anthraquinone at room temperature in a flow cell without the use of hazardous oxidants or noble metal catalysts. The anthraquinone, generated *in situ*, was used as the active species in a flow battery electrolyte without further modification or purification. This potentially scalable, safe, green, and economical electro-synthetic method is also applied to another anthracene-based derivative and may be extended to other redox-active aromatics.

Introduction

Aqueous redox flow batteries (ARFBs) represent a class of devices for storing electrical energy that are especially well suited for large-scale stationary deployment.^{1,2} Vanadium redox flow batteries, the most developed ARFB technology, have been limited by the high and fluctuating price of vanadium.³

Anthraquinone-based aqueous redox flow batteries are considered as one class of the most promising alternatives to vanadium redox flow batteries because they can be composed of earth-abundant elements such as C, H, O, and N while providing comparable electrochemical performance.^{4–9} However, reducing the production cost of anthraquinone-based electrolytes and improving their chemical stability are two major challenges preventing them from being cost-competitive.^{9–14} Many factors can influence the synthesis cost of an organic molecule, including the number, duration, complexity, and yields of the reaction steps, the reaction conditions (time, temperature, and pressure), solvent and precursor costs, the cost of waste disposal, and economies of scale. Likewise, a host of factors contributes to the stability, and by extension the long-term viability, of redox-active organics including the chemical structure, solvent conditions, applied potentials, and state of charge. Only through careful consideration of all of these

factors can commercial-scale organic ARFBs be viable storage solutions. Therefore, not only is the development of a stable anthraquinone important, but the design of a potentially economical, scalable, and green synthetic route toward targeted molecules is equally significant.^{11,15}

Electrochemically-mediated synthesis (electrosynthesis) enables the replacement of hazardous oxidizing and reducing agents by electric current, or “clean” electrons, through an electrode and has attracted considerable attention for both laboratory and industrial applications in multiple fields of research.^{16–21} Compared to traditional thermochemical synthesis, electrosynthesis can be significantly more environmentally benign due to reduced waste production and alternative chemicals consumed.^{22,23} However, the necessity of using specific solvents combined with supporting electrolytes, along with their subsequent separations, are some of the primary hurdles limiting the feasibility of electrosynthesis compared to thermochemical processes in many cases.¹⁶

As an example, anthraquinone is typically produced from anthracene, an inexpensive and abundant component of coal tar and petroleum.²⁴ Typically, hazardous oxidants such as cerium(IV), chromium(VI), and vanadium(V) compounds dissolved in strong acids, sometimes at elevated temperatures, are used to facilitate this thermochemical conversion.²⁵ To minimize the use of hazardous materials, often these consumed oxidants are electrochemically regenerated and reused for chemical oxidations,^{25–30} that is, a mediated or indirect electrochemical oxidation. However, in both thermochemical conversion and mediated (indirect) electrochemical conversion, isolating anthraquinone from these hazardous solutions can be time- and capital-intensive. Electro-oxidations of anthracene and its derivatives at ~1 mM concentration have been performed previously; however, the low concentrations of anthracene substrates and poor selectivity of the reactions

^aDepartment of Chemistry and Chemical Biology, Harvard University, Cambridge, Massachusetts 02138, USA. E-mail: gordon@chemistry.harvard.edu

^bJohn A. Paulson School of Engineering and Applied Sciences, Harvard University, Cambridge, Massachusetts 02138, USA. E-mail: maziz@harvard.edu

^cDepartment of Physics, Harvard University, Cambridge, Massachusetts 02138, USA

†Electronic supplementary information (ESI) available. See DOI: 10.1039/d0gc02236e

‡These authors contributed equally to this work.

have prevented the method from being synthetically useful.^{31–36}

Using a scalable flow cell setup,³⁷ we demonstrate the capability to electrochemically oxidize water-soluble anthracenes directly to anthraquinones in electrolytes without the use of strong oxidants or catalysts, producing the desired negolyte (negative electrolyte) and ferrocyanide posolyte (positive electrolyte) *in situ*. Compared to conventional thermochemical and electrochemical methods, the new method is safe and potentially inexpensive because it eliminates both the use of hazardous oxidants and the necessity of post-synthesis isolation of the products from the supporting electrolytes. Taking advantage of a flow cell and bulk electrolysis setup, the demonstrated electrochemical method is amenable to both continuous and batch processing. Furthermore, we confirmed that the electrochemical method can also be extended to other anthracene derivatives.

3,3'-(9,10-Anthraquinone-diyl)bis(3-methylbutanoic acid) (DPivOHAQ) was recently reported as an extremely stable and potentially inexpensive negolyte active species for organic ARFBs.³⁸ However, the use of CrO₃ in the synthesis can be highly toxic and explosive if produced in large scale. Fig. 1a shows the synthetic route for DPivOHAQ in three steps: (1) through Birch reduction, anthracene (AC) is converted to 9,10-dihydroanthracene (DHAC) at room temperature (Fig. S1†). (2) After a Friedel–Crafts reaction and subsequent oxidation by air in one pot, two water-soluble groups are introduced and DHAC

is re-oxidized to an AC derivative (Fig. S2†), forming 3,3'-(anthracene-diyl)bis(3-methylbutanoic acid) (DPivOHAC). The DPivOHAC powder was then dissolved in water by adding KOH to deprotonate the carboxylic acid groups. (3) Lastly, DPivOHAQ negolyte active species is produced by electrochemical oxidation in an aqueous electrolyte without the need for further purification. Fig. 1b illustrates how DPivOHAQ and ferrocyanide active species can be produced *in situ* in the flow cell's electrochemical mode. These materials can directly serve as the active species in the negolyte and the posolyte, respectively, of a flow battery in the same cell as illustrated in Fig. 1c.

Fig. 2a lists three different oxidation methods for DPivOHAQ synthesis. Conventionally, anthracene derivatives can be chemically oxidized to their anthraquinone forms by oxidants such as chromium oxide (CrO₃) in strong acidic media at elevated temperature.³⁸ To minimize the use of hazardous oxidants, the strategy of mediated electrochemical oxidation can be performed by regenerating oxidants such as cerium(IV) compounds.^{26,29} However, in both of these thermochemical and indirect electrochemical oxidation processes, tedious and expensive isolation of anthraquinone-based products from oxidants and acids is required. Taking advantage of the high solubility of DPivOHAC in base, we demonstrate a synthetic route *via* direct electrochemical oxidation in alkaline electrolyte with a flow cell. This method allows the complete elimination of hazardous oxidants and costly separation processes.

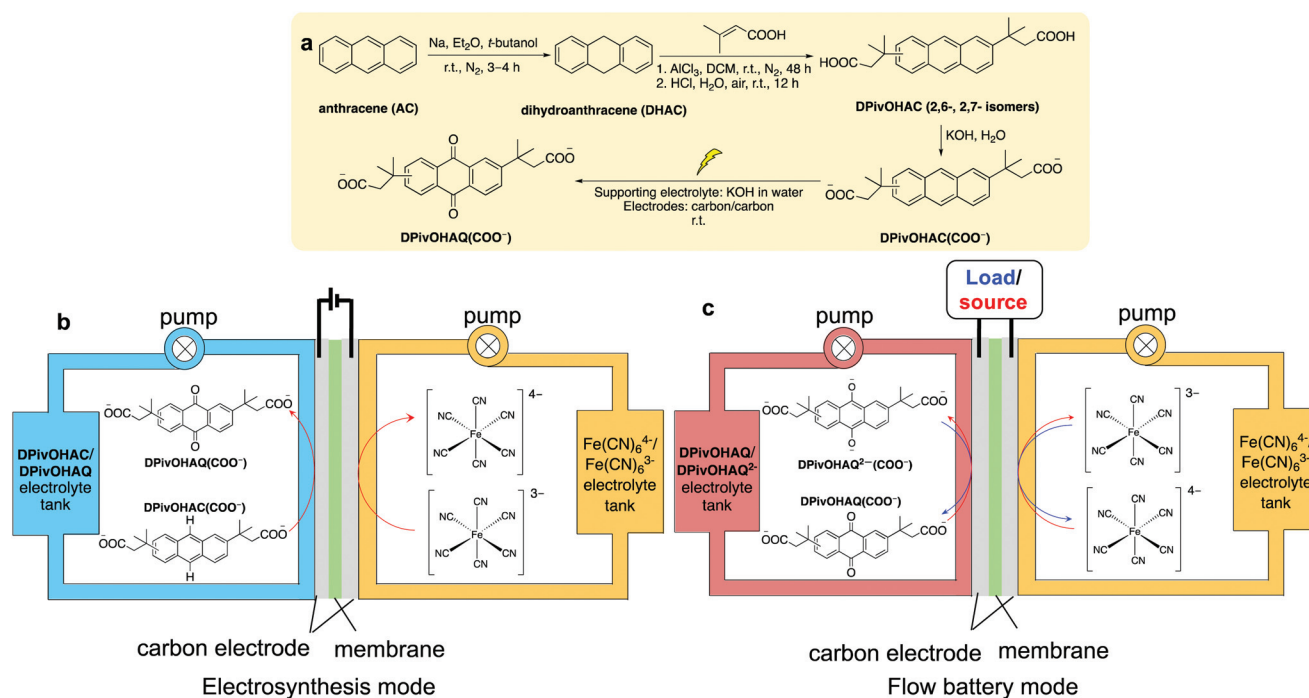


Fig. 1 Preparation of DPivOHAQ and the corresponding flow battery. (a) The DPivOHAQ synthetic route and conditions starting from anthracene. (b) The setup for electrochemical synthesis of DPivOHAQ and ferrocyanide. (c) The flow battery setup with DPivOHAQ negolyte (generated *in situ*) and ferrocyanide posolyte (generated *in situ*). DPivOHAC: 3,3'-(anthracene-diyl)bis(3-methylbutanoic acid); DPivOHAC(COO⁻) is deprotonated DPivOHAC. DPivOHAQ: 3,3'-(9,10-anthraquinone-diyl)bis(3-methylbutanoic acid); DPivOHAQ(COO⁻) is deprotonated DPivOHAQ.

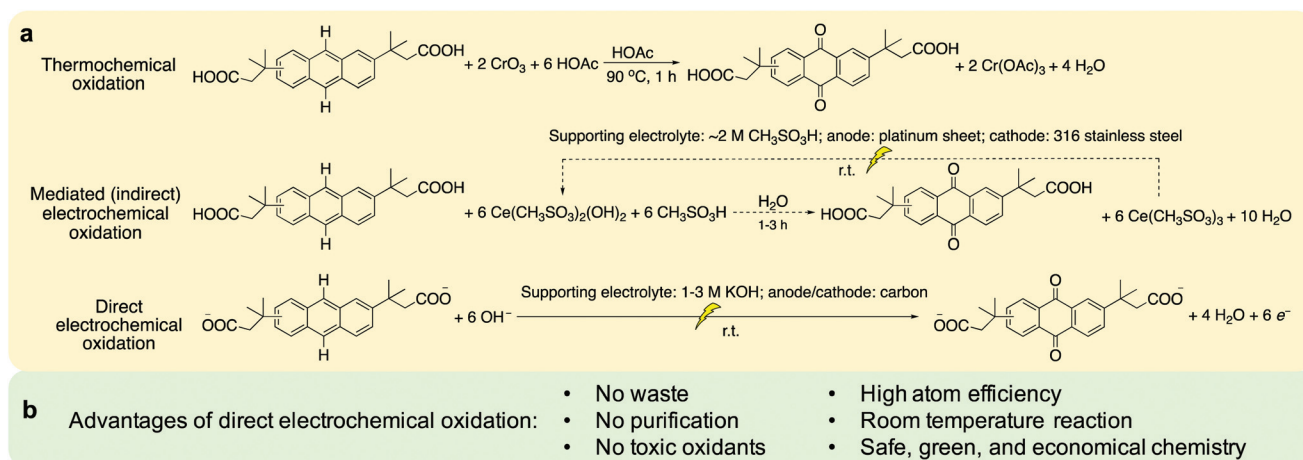


Fig. 2 Comparison of DPivOHAQ synthetic methods. (a) Thermochemical, mediated (indirect) electrochemical, and direct electrochemical oxidation reactions to synthesize DPivOHAQ. (b) Advantages of direct electrochemical oxidation *in situ*.

Experimental

Cell hardware

Glassy carbon was used as the working electrode for all three-electrode cyclic voltammetry (CV) tests with a 5 mm diameter glassy carbon working electrode, an Ag/AgCl reference electrode (BASi, pre-soaked in 3 M NaCl solution), and a graphite counter electrode. Both an undivided cell and a divided cell were built for electrosynthesis. Flow battery experiments were constructed with cell hardware from Fuel Cell Tech (Albuquerque, NM) assembled into a zero-gap flow cell configuration. Pyrosealed POCO graphite flow plates with serpentine flow patterns were used for both electrodes. Each electrode comprised a 5 cm² geometric surface area covered by AvCarb HCBA woven carbon fiber without pretreatment, or Pt-coated Toray carbon paper without pretreatment. The membrane is pre-soaked (1 M KOH for 24 hours) Nafion 212.

Undivided electrolytic cell setup (electrochemical oxidation vs. the HER)

Working electrode: carbon felt, where DPivOHAC(COO⁻) was oxidized to DPivOHAQ(COO⁻); counter electrode: carbon rod, where water was reduced to hydrogen gas. While the electrolyte was stirred, a constant potential (1.1 V vs. Ag/AgCl) was applied to the divided electrolytic cell until 120% of the required coulombs were extracted from the working electrode.

Divided electrolytic cell setup (electrochemical oxidation vs. the ORR)

Anode: Commercial AvCarb HCBA (woven carbon cloth), where DPivOHAC(COO⁻) was oxidized to DPivOHAQ(COO⁻); cathode: platinum coated Toray carbon paper, where humidified air/oxygen was reduced to hydroxide. A constant voltage (1.8 V) was applied to the divided electrolytic cell until the current decreased to 2 mA cm⁻². The number of extracted electrons was ~1.2 times higher than the theoretical value.

Divided electrolytic cell setup (electrochemical oxidation vs. the reduction of ferricyanide)

Anode: AvCarb HCBA (woven carbon cloth), where DPivOHAC(COO⁻) was oxidized to DPivOHAQ(COO⁻); cathode: AvCarb HCBA (woven carbon cloth), where potassium ferricyanide was reduced to potassium ferrocyanide. A constant current density (20 mA cm⁻²) was applied to the divided cell for at most 1.5 hours with a 1.2 V voltage cutoff; when either time or voltage reached the limit, the potential was held (1.2 V vs. ferro-/ferricyanide) until the current decreased to 2 mA cm⁻². The number of extracted electrons was ~1.2 times higher than the theoretical value.

An aliquot (~250 μL) was transferred from the as-prepared anolyte to an Eppendorf® tube (capacity: 1.5 mL) and acidified by a drop of concentrated HCl to obtain DPivOHAQ precipitate. The final DPivOHAQ precipitate was re-dissolved in DMSO-*d*₆ for ¹H NMR measurement. The yield was determined by peak integrations of the spectrum. Faradaic efficiency (%) = yield (%) / 1.2. More detailed information can be found in the ESI.†

Results and discussion

In an electrolytic cell, an anodic oxidation half reaction must be accompanied by a cathodic reduction half reaction. As shown in Table 1, we devise three different reduction half reactions to be coupled with direct DPivOHAC electrochemical oxidation, *i.e.*, the hydrogen evolution reaction (HER), the oxygen reduction reaction (ORR), and the Fe(CN)₆³⁻ to Fe(CN)₆⁴⁻ reduction reaction. The corresponding oxidation or reduction potentials for these reactions are listed in Table 1.

For the electrochemical oxidation of DPivOHAC to DPivOHAQ, two cell types are used, as diagrammed and described in Fig. S3 and S4.† A divided cell uses an ion exchange membrane to separate the two half reactions, resem-

Table 1 Anodic, cathodic, and overall reactions for direct electrochemical oxidation

Reactions	Potential at pH 14 (V vs. SHE)/cell voltage (V)
Anodic	
$\text{DPivOHAC}(\text{COO}^-) + 6 \text{OH}^- \rightarrow \text{DPivOHAQ}(\text{COO}^-) + 4 \text{H}_2\text{O} + 6 \text{e}^-$	1.14 ^a
Cathodic	
$6 \text{H}_2\text{O} + 6 \text{e}^- \rightarrow 3 \text{H}_2 + 6 \text{OH}^-$ (divided or undivided cell)	-0.83
$1.5 \text{O}_2 + 6 \text{e}^- + 3 \text{H}_2\text{O} \rightarrow 6 \text{OH}^-$ (divided or undivided cell)	0.40
$6 \text{Fe}(\text{CN})_6^{3-} + 6 \text{e}^- \rightarrow 6 \text{Fe}(\text{CN})_6^{4-}$ (divided cell)	0.44
Overall	
$\text{DPivOHAC}(\text{COO}^-) + 2 \text{H}_2\text{O} \rightarrow \text{DPivOHAQ}(\text{COO}^-) + 3 \text{H}_2$	1.97
$\text{DPivOHAC}(\text{COO}^-) + 1.5 \text{O}_2 \rightarrow \text{DPivOHAQ}(\text{COO}^-) + \text{H}_2\text{O}$	0.74
$\text{DPivOHAC}(\text{COO}^-) + 6 \text{OH}^- + 6 \text{Fe}(\text{CN})_6^{3-} \rightarrow \text{DPivOHAQ}(\text{COO}^-) + 6 \text{Fe}(\text{CN})_6^{4-} + 4 \text{H}_2\text{O}$	0.70

^aThe electro-oxidation potential at peak current.

bling the architecture of traditional fuel cells and ARFBs. An undivided cell employs two electrodes suspended in electrolyte without the use of a membrane, reflecting a bulk electrolysis cell.

Comparing these three overall reactions, the first one paired with the HER requires the highest voltage; the second one paired with the ORR is known to have slow reaction kinetics and a high overpotential;³⁹ the third one paired with $\text{Fe}(\text{CN})_6^{3-}$ to $\text{Fe}(\text{CN})_6^{4-}$ reduction exhibits the lowest overall reaction cell voltage, suggesting the least amount of energy will be required for electrosynthesis. Another merit of the third reaction is the *in situ* generation of the desired negolyte active species (**DPivOHAQ**) and posolyte active species $\text{Fe}(\text{CN})_6^{4-}$ simultaneously. The disadvantage is that at least six equivalents of ferricyanide and hydroxide are used. Given the similar reduction potentials of the ORR and of ferricyanide to ferrocyanide, an important direction for future research is the concurrent reduction of oxygen and ferricyanide in order to achieve high yields as well as lower ferricyanide usage. By using the same full cell configuration without changing electrolyte reservoirs, carbon-based electrodes, or ion-exchange membranes, we can immediately switch from electrosynthesis mode to flow battery mode for electrochemical energy storage. In this configuration, neither hazardous oxidants nor purification steps are needed, nor is waste generated. Furthermore, the reaction may proceed at room temperature with high atom efficiency. The new synthesis is therefore potentially safe, green, economical, and scalable.

The cyclic voltammogram (CV) of **DPivOHAC** at pH 14 (Fig. 3a) indicates a peak oxidation current at 1.14 V vs. SHE. This value is more positive than the standard redox potential of 0.40 V vs. SHE for the oxygen evolution reaction (OER), and we expect that the OER will be a major side reaction of electrosynthesis.

We then assembled a flow cell with **DPivOHAC** as the anolyte and $\text{K}_3\text{Fe}(\text{CN})_6$ as the catholyte. Galvanostatic electrolysis with a potentiostatic hold after reaching a potential limit of 1.2 V was performed for ~4.5 hours to complete the electrosynthesis. The OER side reaction, evidenced by the observation of bubbles generated in the anolyte, precludes a faradaic efficiency of 100%. Thus, the number of electrons extracted from the anolyte was ~1.2 times higher than the theoretical number for complete conversion. A plateau appears at ~0.8 V

against $\text{K}_3\text{Fe}(\text{CN})_6$ (0.44 V vs. SHE) in the voltage profile (Fig. 3b).

We compared the CV of **DPivOHAQ** produced by electrosynthesis against the reduction of $\text{Fe}(\text{CN})_6^{3-}$ to that of the chemically synthesized product at the same concentration to verify that the reaction products are the same regardless of the synthetic procedure employed (Fig. 3c). The two CV curves show identical redox peaks and similar peak currents, indicating a high-yield electrosynthesis process. ¹H nuclear magnetic resonance (NMR) spectroscopy was used to further examine the structure of electrosynthesized **DPivOHAQ** when using either a divided or undivided cell (Fig. S3†) and to compare the spectra with those of the starting material, **DPivOHAC**, and the chemically synthesized **DPivOHAQ**. The top three spectra in Fig. 3d are the ¹H NMR spectra from electrosynthesized **DPivOHAQ**, in which the dominant peaks have the same chemical shifts as those in the spectrum of chemically synthesized **DPivOHAQ**, further suggesting the desired product was achieved.

Slightly different yields of **DPivOHAQ** were obtained when paired with the HER in an undivided cell or with $\text{Fe}(\text{CN})_6^{3-}$ reduction or the ORR in a divided cell (Fig. S4†). The 82.7% yield when paired with the HER in an undivided cell could be explained by a molecular shuttling effect; *i.e.*, the electrosynthesized **DPivOHAQ** can first migrate to the cathode where it is reduced, then diffuse back to the anode for re-oxidation. As a result, double counting of electrons can occur. When paired with the $\text{Fe}(\text{CN})_6^{3-}$ reduction half reaction, a yield of 93.0% was obtained. The incomplete yield is likely due to the consumption and therefore decreased concentration of both **DPivOHAC** and OH^- as the electrosynthesis continues, making further oxidation increasingly difficult.

The use of the ORR half reaction achieved almost 100.0% yield. This exceptional yield may be attributed to the as-formed OH^- ions on the cathode (ORR) side crossing over to the anolyte and compensating for any loss of OH^- ions on the anode side. Overall yields in excess of 80.0% for all three conditions exceed many conventional reactions and are acceptable for direct flow battery use without purification or separation.

To demonstrate the feasibility of switching from the electrosynthesis mode (when paired with $\text{Fe}(\text{CN})_6^{3-}$ reduction) to flow battery mode, we began charge–discharge cycling immediately upon completion of the electrosynthesis, without performing

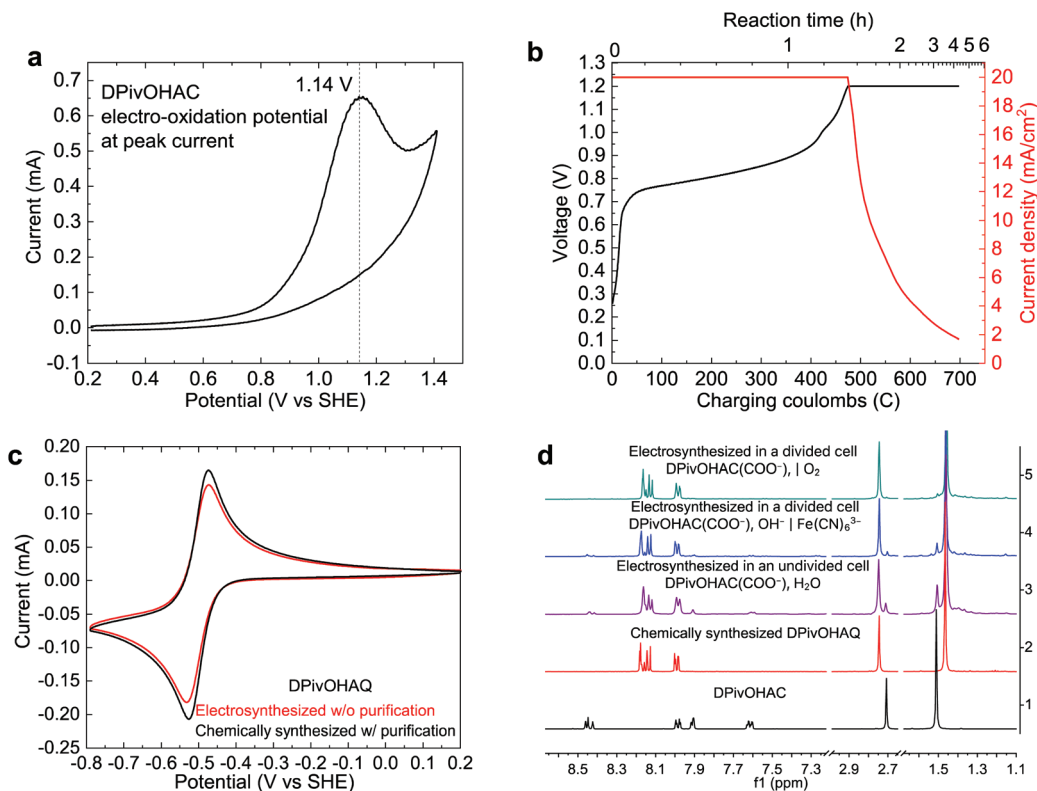


Fig. 3 Electrolysis and characterization of DPivOHAC. (a) The cyclic voltammogram (CV) of 0.1 M DPivOHAC in 1.0 M KCl + 1.0 M KOH aqueous solution. Scan rate: 0.1 V s^{-1} . (b) The electrochemical oxidation was conducted by using a constant current (20 mA cm^{-2}) with a subsequent potential hold (1.2 V) until the current density decreased to 2 mA cm^{-2} . (c) CV of 10 mM electro-synthesized DPivOHAQ (against $\text{Fe}(\text{CN})_6^{3-}$) without purification and 10 mM chemically synthesized DPivOHAQ with purification in 1 M KOH aqueous solutions, respectively. Scan rate: 0.1 V s^{-1} . (d) ^1H NMR spectra of (bottom to top): chemically synthesized DPivOHAC (black); chemically synthesized DPivOHAQ (red); electro-synthesized DPivOHAQ in an undivided cell (purple), 17.3% of DPivOHAC remained unreacted according to the integration, yield: 82.7%; electro-synthesized DPivOHAQ in a divided cell against $\text{Fe}(\text{CN})_6^{3-}$ (blue), 7.0% of DPivOHAC remained unreacted according to the integration, yield: 93.0%; electro-synthesized DPivOHAQ in a divided cell against O_2 (green), 0% of DPivOHAC remained unreacted according to the integration, yield: 100%. The deuterated solvent is $\text{DMSO}-d_6$, and the solvent peaks (DMSO and H_2O) were removed to better display the peaks of interest. The electro-synthetic details are described under the headings **Electrosynthesis I**, **II**, and **III** in the ESI.†

any purification. Because other research has reported that quinones and related compounds can decompose in the presence of light,^{40–42} we wrapped the electrolyte reservoirs with aluminum foil to avoid light-induced decomposition during cell cycling (Fig. S13–S15†). Fig. 4a shows the charge–discharge profile of a single cycle with an open circuit voltage of $\sim 1.0 \text{ V}$ and a capacity of 84.0 coulombs. Given the 93.0% yield found from the ^1H NMR, the capacity utilization is 93.6%. Long-term cycling was then performed to determine a temporal capacity fade rate of the full cell. Fig. 4b demonstrates the discharge capacity and coulombic efficiency over 33.2 days and 2271 cycles with a fitted fade rate of 0.014% per day and an average coulombic efficiency of 99.53%. This is consistent with the fade rate of chemically synthesized DPivOHAQ.³⁸ The extremely low capacity fade rate is attributed to the chemical stability of the molecular structure. The C–C covalent bond between the anthraquinone core and the functionalizing chains is more robust in strong base and at elevated temperature than the C–O bond demonstrated in previous work.^{4,5,38} Furthermore, the two branched methyl groups on the carbon

connected to the anthraquinone (AQ) core may increase the stability of the solubilizing chain even when exposed to harsh conditions.¹⁵

To examine the feasibility of this method for potential industry use, we further conducted electro-synthesis with a higher concentration (0.5 M) of DPivOHAC at a higher current density (100 mA cm^{-2}) (see Fig. S5†). Fig. 4c shows that 0.5 M electro-synthesized negolyte can deliver 72.9% of the theoretical capacity. We attribute the discrepancy between the delivered capacity and the theoretical capacity primarily to incomplete conversion (Fig. S6†). The capacity utilization is 81.9% if we consider that there is 11.0% unreacted DPivOHAC(COO[−]) in the negolyte. Additionally, the mass transport of active species at 0.5 M concentration may be another issue limiting the full capacity utilization. The corresponding polarization curve at different states of charge (SOC) is shown in Fig. 4d. The peak power density exceeds 0.2 W cm^{-2} when at $\sim 100\%$ of SOC.

Given the total transfer of six electrons during the electro-synthesis of DPivOHAC to DPivOHAQ, the high yields achieved

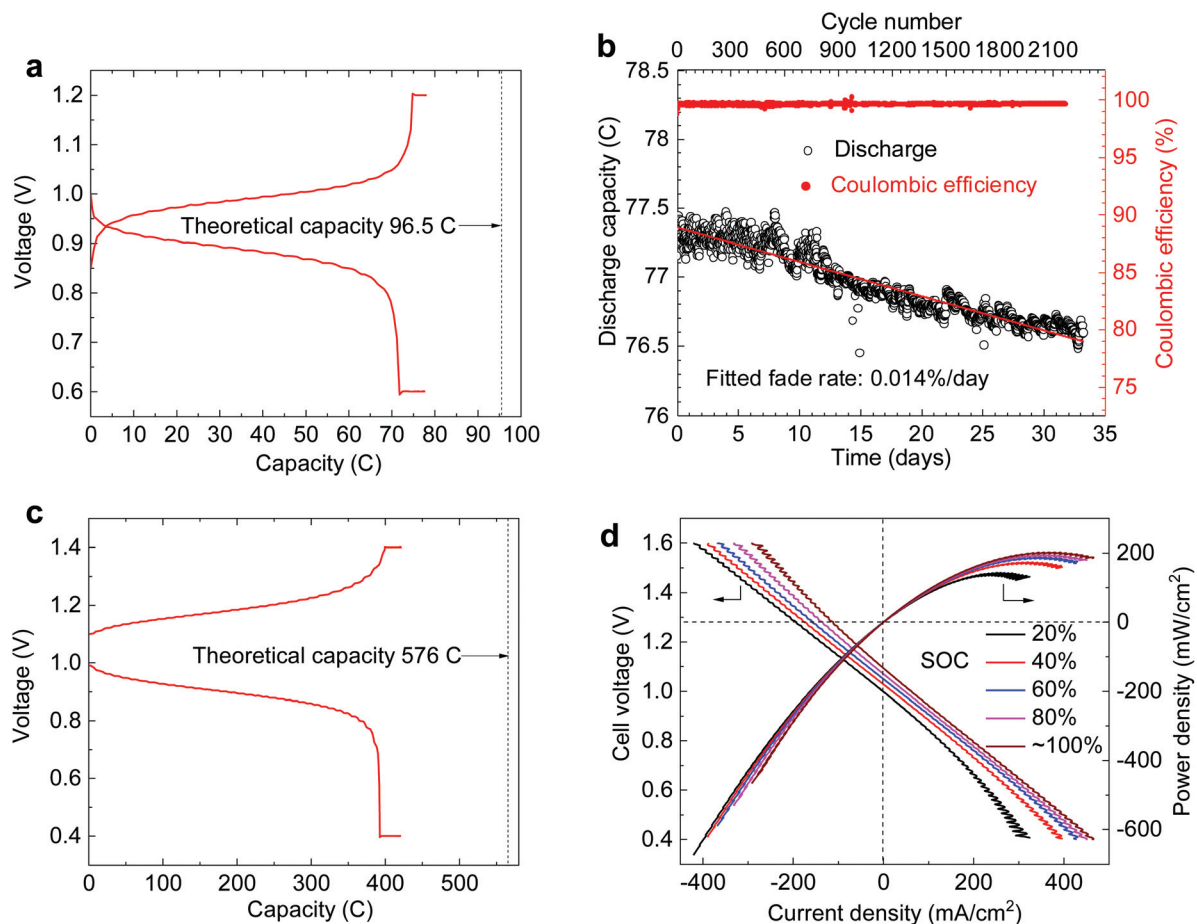
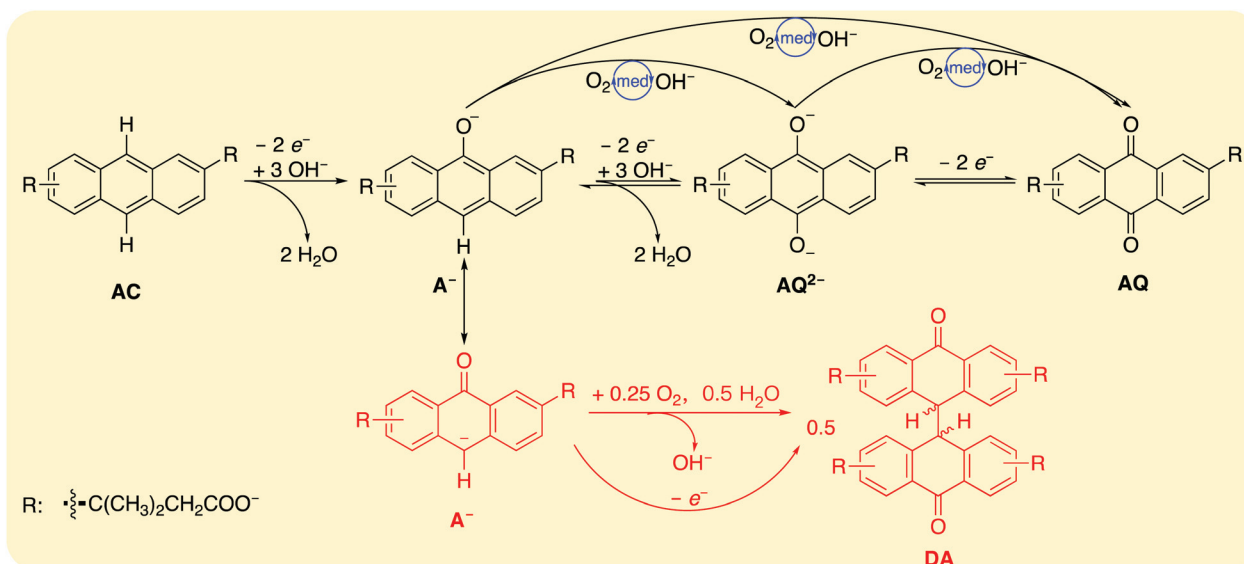


Fig. 4 Full cell performance evaluation from Electrosynthesis III and IV. (a) A representative charge–discharge profile with 0.1 M DPivOHAQ. Negolyte: 5 mL of 0.1 M DPivOHAQ, pH = ~13.5. Posolyte: 100 mL of 0.1 M potassium ferro-/ferricyanide solution [~ 0.06 M $K_4Fe(CN)_6$ and ~ 0.04 M $K_3Fe(CN)_6$], pH = ~13.6. (b) Discharge capacity (C) and coulombic efficiency (%) vs. cycle number and time (days). Negolyte: 4.5 mL of 0.1 M DPivOHAQ. Posolyte: 100 mL of 0.1 M ferro-/ferricyanide solution [~ 0.06 M $K_4Fe(CN)_6$ and ~ 0.04 M $K_3Fe(CN)_6$]. Current density: 30 mA cm^{-2} with potential hold (cutoffs: 0.6 V, 1.2 V) until current decreased to 2 mA cm^{-2} . (c) A representative charge–discharge profile with 0.5 M DPivOHAQ. Negolyte: 6 mL of 0.5 M DPivOHAQ. Posolyte: 100 mL of 0.5 M potassium ferro-/ferricyanide solution [~ 0.3 M $K_4Fe(CN)_6$ and ~ 0.2 M $K_3Fe(CN)_6$]. Current density: 100 mA cm^{-2} with potential hold (cutoff: 0.4 V, 1.4 V) until current decreased to 2 mA cm^{-2} . (d) Polarization curves of the 0.5 M DPivOHAQ at the SOC of 20%, 40%, 60%, 80%, and ~100% respectively. Descriptions of Electrosynthesis III and IV can be found in the ESI.†

in this work might be surprising. We hypothesize a three-step successive two-electron transfer mechanism (Scheme 1):^{34,35} first, when a potential is applied, anthracene (AC) may react with three OH^- ions and donate two electrons to produce two water molecules and the anthrone anion (A^-); second, A^- may further react with another three OH^- ions and donate another two electrons to generate two water molecules and the deprotonated anthrahydroquinone dianion (AQ^{2-}); third, AQ^{2-} may further release two electrons to afford the anthraquinone species (AQ). Complete electrochemical conversion in the third step has been well-documented at negative potentials vs. ferro-/ferricyanide,^{1,2,43} and should therefore be rapid at positive potentials vs. ferro-/ferricyanide. The reverse reaction of the second step has recently been identified as a side reaction in ARFBs, and the forward reaction is chemically feasible when exposed to O_2 or air.^{14,38} Given the high voltage applied to the cell, it is thus plausible that the forward reactions (AC to

A^- to AQ^{2-} /AQ) can electrochemically proceed completely and swiftly.

Our group has also previously proposed a side reaction pathway for anthraquinones,^{14,44} where the anthrone anion (A^-) can be oxidatively dimerized to dianthrone (DA) chemically and/or electrochemically (Scheme 1). According to 1H NMR spectra (Fig. 3d) and liquid chromatography–mass spectrometry (LC–MS) results (Fig. S7†), neither DA nor Kolbe electrolysis-related byproducts⁴⁵ were detected (Scheme S1†), suggesting that AC/AQ-related side reactions can be negligible when a sufficient OH^- concentration is present to prevent dianthrone formation and a sufficiently low voltage cutoff is chosen to prevent Kolbe electrolysis dimer formation. The major competing side reaction is the OER, which, along with the reactions of AC to A^- to AQ^{2-} , will consume OH^- and may lead to the formation of DA as a result of insufficient OH^- ions in the DPivOHAC solution (see Electrosynthesis V in the ESI†).



Scheme 1 Proposed electrochemical oxidation mechanism. Three-step successive two-electron transfer process from AC to A^- , A^- to AQ^{2-} , and AQ^{2-} to AQ. The generated oxygen from the OER side reaction may incur chemical oxidation processes including A^- to AQ^{2-} , AQ^{2-} to AQ, and oxidative dimerization (A^- to DA).

Interestingly, the dianthrone (Scheme S2†), detected by LC-MS (Fig. S11†), are surprisingly redox-active when a broad voltage window is applied (Fig. S8 and S9 and Scheme S2†). On the one hand, the OER can reduce faradaic efficiency; on the other hand, the generated oxygen can serve as a mediator and chemically oxidize intermediates (*i.e.*, A^- , AQ^{2-}) to the final AQ form, *i.e.*, mediated (indirect) electrochemical oxidation. Because the entire process involves not only electrochemical oxidations, but also chemical oxidations, it is more appropriate to call it an electrochemical–chemical oxidation process.⁴⁶

In the proposed mechanism, the anthrone derivative is an intermediate in the electrochemical oxidation. Anthrone formation has been identified as the major side reaction causing capacity fade in previous work;^{14,38} therefore, it is plausible that lost capacity of anthraquinone flow battery systems may be recovered and anthraquinone lifetime extended by electrochemically oxidizing anthrone to redox-active anthraquinone derivatives.

To demonstrate that the electrochemical oxidation can be applied to other anthracene derivatives, we performed electrochemical oxidation of 4,4'-(9,10-dihydroanthracene-diyl)dibutanoic acid (**DBDHAC**), where the molecular core is 9,10-dihydroanthracene.³⁸ The ¹H NMR results indicate that **DBDHAC** can, like **DPivOHAC**, be electrochemically oxidized to the final anthraquinone (Fig. S12†), **DBAQ** (4,4'-(9,10-anthraquinone-diyl)dibutanoic acid), which has also been shown to be extremely stable.³⁸

The shared precursor of **DPivOHAQ** and **DBAQ**, anthracene, is abundant in crude petroleum and coal tar, and can be synthesized from benzene and benzyl alcohol (Scheme S3†).⁴⁷ The precursor of **DPivOHAQ**, 3,3'-dimethyl acrylic acid, can be industrially produced from malonic acid, a food acid; the pre-

cursor of **DBAQ**, succinic anhydride, can be industrially hydrogenated from maleic anhydride and used as an important intermediate on an industrial scale. Thus, both **DPivOHAQ** and **DBAQ** can be readily synthesized from commodity chemicals. Although the synthetic cost of **DPivOHAQ** or **DBAQ** should be somewhat higher than that of 2,6-dihydroxyanthraquinone (**DHAQ**) due to more steps and more chemicals involved, the capital cost of AORFBs that utilize finite-lifetime electrolytes can be viewed as including the total active cost, which is the sum of the initial cost of redox-active materials and the present value of the future costs of periodic electrolyte replacement.¹³ This can lead to an initial cost–lifetime trade-off in the choice of electrolytes. Over an extended operational lifetime, the total active cost of **DPivOHAQ** or **DBAQ** may be less than that of **DHAQ** due to their much longer lifetimes.¹⁴

Conclusion

This work demonstrates a potentially scalable, safe, green, and economical *in situ* electrochemical method for anthraquinone electrolytes in a flow cell without the use of hazardous oxidants or precious metal catalysts. The as-generated electrolytes, which are extremely stable, can be immediately used in a redox flow battery without separation or purification. Other low-cost compounds may also be amenable to this approach, providing a pathway to lower the cost of electrochemical grid storage systems, thereby accelerating the development of a renewable energy economy. The technique extends the opportunities for direct aqueous electrochemical synthesis to replace thermochemical synthesis of value-added organics.

Conflicts of interest

Harvard University has filed a patent application on the materials and the electrosynthetic methods described in this paper.

Acknowledgements

This research was supported by U.S. DOE award DE-AC05-76RL01830 through PNNL subcontract 428977, Innovation Fund Denmark *via* the Grand Solutions project “ORBATS” file no. 7046-00018B, and NSF grant CBET-1914543. D. A. P. acknowledges funding support from the NSF Graduate Research Fellowship Program, no. DGE1144152 and DGE1745303.

References

- 1 B. Huskinson, M. P. Marshak, C. Suh, S. Er, M. R. Gerhardt, C. J. Galvin, X. Chen, A. Aspuru-Guzik, R. G. Gordon and M. J. Aziz, *Nature*, 2014, **505**, 195–198.
- 2 K. Lin, Q. Chen, M. R. Gerhardt, L. Tong, S. B. Kim, L. Eisenach, A. W. Valle, D. Hardee, R. G. Gordon, M. J. Aziz and M. P. Marshak, *Science*, 2015, **349**, 1529–1532.
- 3 M. Moore, R. Counce, J. Watson and T. Zawodzinski, *J. Adv. Chem. Eng.*, 2015, **5**, 1–3.
- 4 D. G. Kwabi, K. Lin, Y. Ji, E. F. Kerr, M.-A. Goulet, D. De Porcellinis, D. P. Tabor, D. A. Pollack, A. Aspuru-Guzik, R. G. Gordon and M. J. Aziz, *Joule*, 2018, **2**, 1894–1906.
- 5 Y. Ji, M.-A. Goulet, D. A. Pollack, D. G. Kwabi, S. Jin, D. De Porcellinis, E. F. Kerr, R. G. Gordon and M. J. Aziz, *Adv. Energy Mater.*, 2019, **9**, 1900039.
- 6 A. Hollas, X. Wei, V. Murugesan, Z. Nie, B. Li, D. Reed, J. Liu, V. Sprenkle and W. Wang, *Nat. Energy*, 2018, **3**, 508–514.
- 7 C. Wang, X. Li, B. Yu, Y. Wang, Z. Yang, H. Wang, H. Lin, J. Ma, G. Li and Z. Jin, *ACS Energy Lett.*, 2020, **5**, 411–417.
- 8 J. D. Hofmann, F. L. Pfanschilling, N. Krawczyk, P. Geigle, L. Hong, S. Schmalisch, H. A. Wegner, D. Mollenhauer, J. Janek and D. Schröder, *Chem. Mater.*, 2018, **30**, 762–774.
- 9 D. G. Kwabi, Y. Ji and M. J. Aziz, *Chem. Rev.*, 2020, **120**, 6467–6489.
- 10 Z. Yang, L. Tong, D. P. Tabor, E. S. Beh, M.-A. Goulet, D. De Porcellinis, A. Aspuru-Guzik, R. G. Gordon and M. J. Aziz, *Adv. Energy Mater.*, 2018, **8**, 1702056.
- 11 V. Dieterich, J. D. Milshtein, J. L. Barton, T. J. Carney, R. M. Darling and F. R. Brushett, *Transl. Mater. Res.*, 2018, **5**, 034001.
- 12 S. Jin, E. M. Fell, L. Vina-Lopez, Y. Jing, P. W. Michalak, R. G. Gordon and M. J. Aziz, *Adv. Energy Mater.*, 2020, **10**, 1–10.
- 13 F. R. Brushett, M. J. Aziz and K. E. Rodby, *ACS Energy Lett.*, 2020, **5**, 879–884.
- 14 M.-A. Goulet, L. Tong, D. A. Pollack, D. P. Tabor, S. A. Odom, A. Aspuru-Guzik, E. E. Kwan, R. G. Gordon and M. J. Aziz, *J. Am. Chem. Soc.*, 2019, **141**, 8014–8019.
- 15 P. Anastas and N. Eghbali, *Chem. Soc. Rev.*, 2010, **39**, 301–312.
- 16 D. S. P. Cardoso, B. Šljukić, D. M. F. Santos and C. A. C. Sequeira, *Org. Process Res. Dev.*, 2017, **21**, 1213–1226.
- 17 M. Yan, Y. Kawamata and P. S. Baran, *Chem. Rev.*, 2017, **117**, 13230–13319.
- 18 B. K. Peters, K. X. Rodriguez, S. H. Reisberg, S. B. Beil, D. P. Hickey, Y. Kawamata, M. Collins, J. Starr, L. Chen, S. Udyavara, K. Klunder, T. J. Gorey, S. L. Anderson, M. Neurock, S. D. Minteer and P. S. Baran, *Science*, 2019, **363**, 838–845.
- 19 E. J. Horn, B. R. Rosen, Y. Chen, J. Tang, K. Chen, M. D. Eastgate and P. S. Baran, *Nature*, 2016, **533**, 77–81.
- 20 A. Badalyan and S. S. Stahl, *Nature*, 2016, **535**, 406–410.
- 21 G. G. Botte, *Electrochem. Soc. Interface*, 2014, **23**, 49–55.
- 22 P. M. Bersier, L. Carlsson and J. Bersier, *Top. Curr. Chem.*, 1994, **170**, 116–136.
- 23 C. Xia, Y. Xia, P. Zhu, L. Fan and H. Wang, *Science*, 2019, **366**, 226–231.
- 24 M. Granda, C. Blanco, P. Alvarez, J. W. Patrick and R. Menendez, *Chem. Rev.*, 2014, **114**, 1608–1636.
- 25 R. S. Tipson, in *National Bureau of Standards Monograph*, 1965, vol. 87, pp. 1–49.
- 26 R. P. Kreh, R. M. Spotnitz and J. T. Lundquist, *J. Org. Chem.*, 1989, **54**(7), 1526–1531.
- 27 E. Oppermann, *US Pat*, US823435A, 1906.
- 28 E. Steckhan, in *Ullmann's Encyclopedia of Industrial Chemistry*, Wiley-VCH Verlag GmbH & Co. KGaA, Weinheim, 2011, 12, DOI: 10.1002/14356007.o09_o04.
- 29 R. M. Spotnitz, R. P. Kreh, J. T. Lundquist and P. J. Press, *J. Appl. Electrochem.*, 1990, **20**, 209–215.
- 30 R. P. Kreh, R. M. Spotnitz and J. T. Lundquist, *Tetrahedron Lett.*, 1987, **28**, 1067–1068.
- 31 E. J. Majeski, J. D. Stuart and W. E. Ohnesorge, *J. Am. Chem. Soc.*, 1968, **90**, 633–636.
- 32 L. R. Faulkner and A. J. Bard, *J. Am. Chem. Soc.*, 1968, **90**, 6284–6290.
- 33 C. Amatore and A. R. Brown, *J. Am. Chem. Soc.*, 1996, **118**, 1482–1486.
- 34 O. Tovide, N. Jahed, C. E. Sunday, K. Pokpas, R. F. Ajayi, H. R. Makelane, K. M. Molapo, S. V. John, P. G. Baker and E. I. Iwuoha, *Sens. Actuators, B*, 2014, **205**, 184–192.
- 35 C. A. Paddon, C. E. Banks, I. G. Davies and R. G. Compton, *Ultrason. Sonochem.*, 2006, **13**, 126–132.
- 36 V. D. Parker, *Acta Chem. Scand.*, 1970, **24**, 2757–2767.
- 37 T. Noel, Y. Cao and G. Laudadio, *Acc. Chem. Res.*, 2019, **52**, 2858–2869.
- 38 M. Wu, Y. Jing, A. A. Wong, E. M. Fell, S. Jin, Z. Tang, R. G. Gordon and M. J. Aziz, *Chem*, 2020, **6**, 1432–1442.
- 39 R. W. Zurilla, R. K. Sen and E. Yeager, *J. Electrochem. Soc.*, 1978, **125**, 1103–1109.

- 40 G. Maier, L. H. Franz, H.-G. Hartan, K. Lanz and H. P. Reisenauer, *Chem. Ber.*, 1985, **118**, 3196–3204.
- 41 S. A. Carlson and D. M. Hercules, *Anal. Chem.*, 1973, **45**, 1794–1799.
- 42 B. E. Hulme, E. J. Land and G. O. Phillips, *J. Chem. Soc., Faraday Trans. 1*, 1972, **68**, 1992–2002.
- 43 M. Quan, D. Sanchez, M. F. Wasylkiw and D. K. Smith, *J. Am. Chem. Soc.*, 2007, **129**, 12847–12856.
- 44 S. Jin, Y. Jing, D. G. Kwabi, Y. Ji, L. Tong, D. De Porcellinis, M. A. Goulet, D. A. Pollack, R. G. Gordon and M. J. Aziz, *ACS Energy Lett.*, 2019, **4**, 1342–1348.
- 45 H.-J. Schäfer, *Top. Curr. Chem.*, 1990, **152**, 91–151.
- 46 C. Costentin and J.-M. Savéant, *Proc. Natl. Acad. Sci. U. S. A.*, 2019, **116**, 11147–11152.
- 47 H. E. Ungnade and E. W. Crandall, *J. Am. Chem. Soc.*, 1949, **71**, 3009–3010.

Supplementary Information

In situ Electrosynthesis of Anthraquinone Electrolytes in Aqueous Flow Batteries

Yan Jing,¹§ Min Wu,²§ Andrew A. Wong,² Eric M. Fell,² Shijian Jin,² Daniel A. Pollack,³ Emily F. Kerr,¹ Roy G. Gordon,^{*,1,2} Michael J. Aziz^{*,2}

¹ Department of Chemistry and Chemical Biology, Harvard University, Cambridge, Massachusetts 02138, United States

² John A. Paulson School of Engineering and Applied Sciences, Harvard University, Cambridge, Massachusetts 02138, United States

³ Department of Physics, Harvard University, Cambridge, Massachusetts 02138, United States

§ These authors contributed equally to this work.

* Correspondence: gordon@chemistry.harvard.edu; maziz@harvard.edu

Table of Contents

General information for synthesis and characterization.....	3
Electrochemical characterization	3
Brief description of electrosynthesis.....	3
Figure S1. ¹H NMR spectra of commercial and synthesized 9,10-dihydroanthracene (DHAC) in DMSO-<i>d</i>₆.....	4
Figure S2. ¹H NMR spectra of 2,7-, 2,6-DPivOHAC isomers and their mixture (aromatic region) in DMSO-<i>d</i>₆.....	5
Figure S3. Photos of undivided cell (a) and divided cell (b).	5
Figure S4. Schematics of (a) undivided cell against the HER and divided cells against (b) the ORR and (c) ferricyanide to ferrocyanide, respectively. (d) ¹H NMR spectra of (bottom to top): chemically synthesized DPivOHAC (black); chemically synthesized DPivOHAQ (red); electrosynthesized DPivOHAQ in an undivided cell (purple), 17.3% of DPivOHAC remained unreacted according to the integration, yield: 82.7%; electro-synthesized DPivOHAQ in a divided cell against Fe(CN)₆³⁻ (blue), 7.0% of DPivOHAC remained unreacted according to the integration, yield: 93.0%; electrosynthesized DPivOHAQ in a divided cell against O₂ (green), 0 % of DPivOHAC remained unreacted according to the integration, yield: 100%. The deuterated solvent is DMSO-<i>d</i>₆, and the solvent peaks (DMSO and H₂O) were removed to better display the peaks of interest. The electrosynthetic details are described under the headings Electrosynthesis I, II, and III.....	6
Electrosynthesis I. Electrochemical synthesis of DPivOHAQ(COO⁻) in an undivided cell at 0.1 M concentration, against the hydrogen evolution reaction (HER).	7

36	Electrosynthesis II. Electrochemical synthesis of DPivOHAQ(COO ⁻) in a divided cell at 0.1 M concentration, against the oxygen reduction reaction (ORR).	8
37		
38	Electrosynthesis III. Electrochemical synthesis of DPivOHAQ(COO ⁻) in a divided cell at 0.1 M concentration, against the reduction of ferricyanide.....	8
39		
40	Electrosynthesis IV. Electrochemical synthesis of DPivOHAQ(COO ⁻) in a divided cell at 0.5 M concentration with excess hydroxide, against the reduction of ferricyanide.	9
41		
42	Figure S5. The electrochemical oxidation of 0.5 M DPivOHAC(COO ⁻) (Electrosynthesis IV). ...	10
43	Figure S6. ¹ H NMR spectrum of DPivOHAQ in DMSO- <i>d</i> ₆ synthesized via the procedure described in Electrosynthesis IV	11
44		
45	Figure S7. Mass spectra of partially electrosynthesized DPivOHAQ (from Electrosynthesis IV) measured by liquid chromatography–mass spectrometry (LC–MS).	12
46		
47	Scheme S1. Kolbe electrolysis.....	13
48	Electrosynthesis V. Electrochemical synthesis of DPivOHAQ(COO ⁻) in a divided cell at 0.5 M concentration with a stoichiometric quantity of hydroxide, against the reduction of ferricyanide.	13
49		
50	
51	Formation of dianthrone during electrosynthesis.....	14
52	Figure S8. Cell performance of 0.5 M electrosynthesized DPivOHAQ when a stoichiometric quantity of hydroxide was added into the DPivOHAC(COO ⁻) solution (Electrosynthesis V).	14
53		
54	Figure S9. Voltage profiles of 0.5 M electrosynthesized DPivOHAQ when a stoichiometric quantity of hydroxide was added into the DPivOHAC solution (Electrosynthesis V) with different lower voltage cutoffs [(a) 0.6, (b) 0.2, (c) 0.6, and (d) 0.7 V].	15
55		
56		
57	Figure S10. ¹ H NMR spectrum of cycled 0.5 M electrosynthesized DPivOHAQ when a stoichiometric quantity of hydroxide was added into the DPivOHAC(COO ⁻) solution (Electrosynthesis V).	16
58		
59		
60	Figure S11. LC–MS results of cycled 0.5 M electrosynthesized DPivOHAQ when a stoichiometric quantity of hydroxide was added into the DPivOHAC solution (Electrosynthesis V).	17
61		
62	Electrosynthesis VI. Electrochemical synthesis of DBAQ(COO ⁻) in an undivided electrolytic cell at 0.1 M concentration, against the HER.	18
63		
64	Figure S12. ¹ H NMR spectra of DBDHAC (bottom), chemically synthesized DBAQ (top), and electrochemically synthesized DBAQ in an undivided cell after varying extents of reaction.....	19
65		
66	Light sensitivity experiments.....	19
67	Figure S13. Samples of (a) DPivOHAQ (0.1 M, pH 12) stored for 1 week in the absence of light (– hv) and under a 500 W lamp (+ hv) and of (b) DBAQ (0.1 M, pH 12) stored for 1 week in the absence of light (– hv) and under a 500 W lamp (+ hv)	20
68		
69		

70 **Figure S14. ¹H NMR spectra of samples of DPivOHAQ (0.1 M, pH 12) stored for 1 week in the**
71 **absence of light (– hν) and under a 500 W lamp (+ hν), each diluted (1:5.5) in pH 14 D₂O (1 M**
72 **KOD) containing a 9 mM NaCH₃SO₃ internal standard (.....21**

73 **Figure S15. ¹H NMR spectra of samples of DBAQ (0.1 M, pH 12) stored for 1 week in the absence**
74 **of light (– hν) and under a 500 W lamp (+ hν), each diluted (1:5) in pH 12 D₂O or in DMSO-*d*₆..22**

75 **Complete synthesis.....23**

76 **Scheme S3. Complete synthetic routes, conditions, and yields of DPivOHAQ and DBAQ when**
77 **commercially available commodity chemicals are used as starting materials.23**

78 **Figure S16. ¹H NMR spectra of commercial and synthesized anthracene (AC) in DMSO-*d*₆. The**
79 **peak at 7.37 ppm in the synthesized AC spectrum is from benzene.23**

80

81 **General information for synthesis and characterization**

82 All reagents were purchased from Sigma-Aldrich or Alfa Aesar and used as received unless
83 otherwise stated. All reactions sensitive to moisture or oxygen were carried out in oven-dried or
84 flame-dried and nitrogen-charged glassware. All anhydrous solvents were saturated with argon
85 and passed through a column of activated alumina immediately prior to use.

86

87 ¹H NMR spectra were recorded on Varian INOVA 500 spectrometers at 500 MHz. NMR spectra
88 were recorded in solutions of deuterated dimethyl sulfoxide (DMSO-*d*₆) with the residual dimethyl
89 sulfoxide (δ 2.25 ppm for ¹H NMR), or deuterated water (D₂O) with the residual H₂O (δ 4.79 ppm
90 for ¹H NMR).

91

92 LC–MS was conducted on a Bruker microTOF-Q II mass spectrometer. The sample was diluted
93 by water/acetonitrile (V/V = 1:1) to the desired concentration (~20 μM) before LC–MS
94 measurements.

95

96 **Electrochemical characterization**

97 *Cyclic voltammetry measurements*

98 Glassy carbon was used as the working electrode for all three-electrode CV tests with a 5 mm
99 diameter glassy carbon working electrode, an Ag/AgCl reference electrode (BASi, pre-soaked in
100 3 M NaCl solution), and a graphite counter electrode.

101 All electrochemical oxidation and flow cell cycling was conducted with Biologic equipment and
102 corresponding software.

103

104 *Flow cell setup*

105 Flow battery experiments were constructed with cell hardware from Fuel Cell Tech (Albuquerque,
106 NM) assembled into a zero-gap flow cell configuration. Pyrosealed POCO graphite flow plates
107 with serpentine flow patterns were used for both electrodes. Each electrode comprised a 5 cm²
108 geometric surface area covered by a piece of AvCarb HCBA woven carbon fiber. The membrane
109 is pre-soaked (1 M KOH for 24 hours) Nafion 212.

110

111 **Brief description of electrosynthesis**

112 *Undivided electrolytic cell setup*

113 Working electrode: carbon felt, where **DPivOHAC(COO⁻)** was oxidized to **DPivOHAQ(COO⁻)**;
114 counter electrode: carbon rod, where water was reduced to hydrogen gas.

115

116 *Divided electrolytic cell setup vs. the ORR*

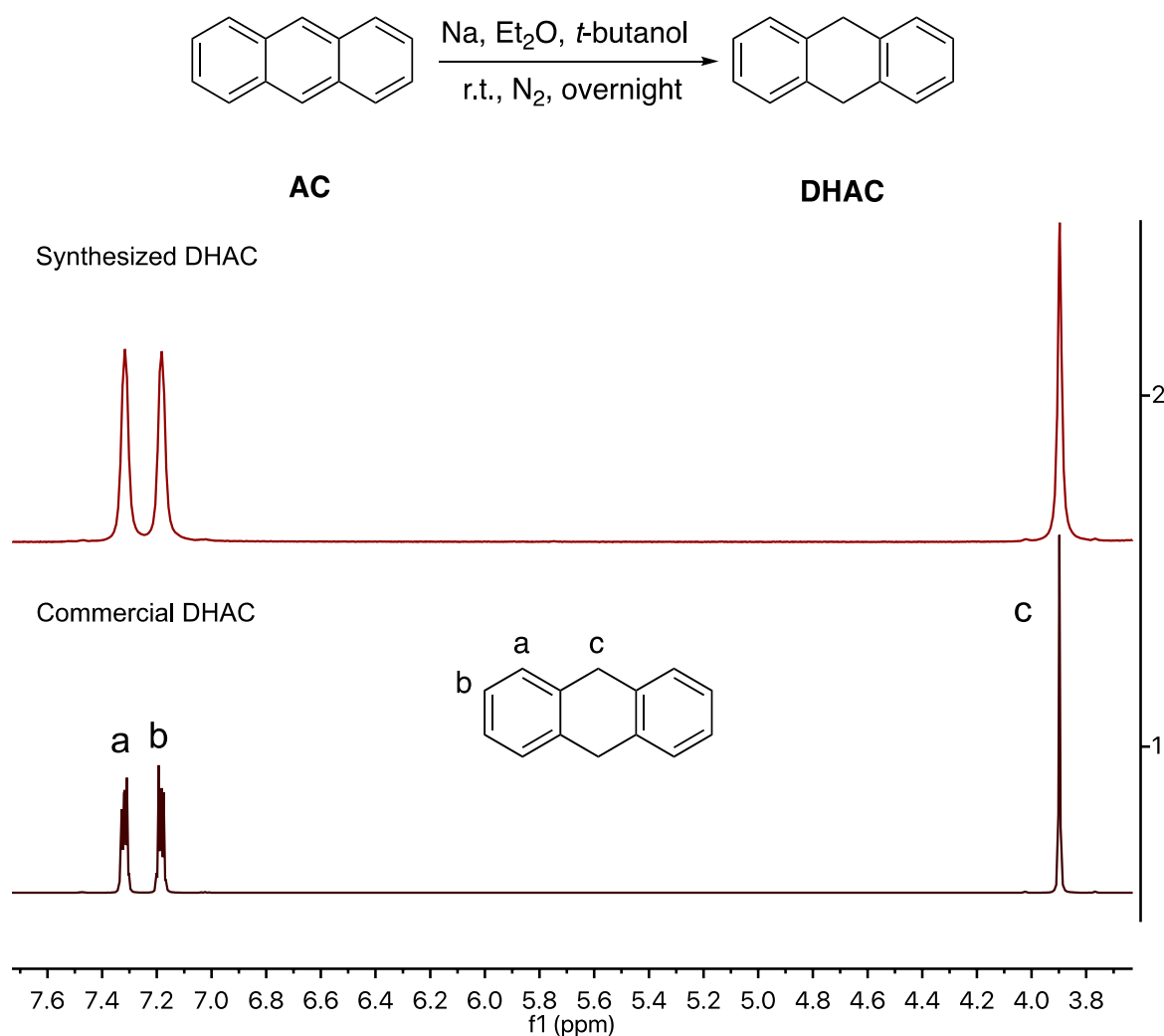
117 Anode: Commercial AvCarb HCBA (woven carbon cloth), where **DPivOHAC(COO⁻)** was
118 oxidized to **DPivOHAQ(COO⁻)**; cathode: platinum coated carbon paper (SGL 39AA), where
119 humidified air/oxygen was reduced to hydroxide.

120

121 *Divided electrolytic cell setup vs. the reduction of ferricyanide*

122 Anode: AvCarb HCBA (woven carbon cloth), where **DPivOHAC(COO⁻)** was oxidized to
123 **DPivOHAQ(COO⁻)**; cathode: AvCarb HCBA (woven carbon cloth), where potassium
124 ferricyanide was reduced to potassium ferrocyanide.

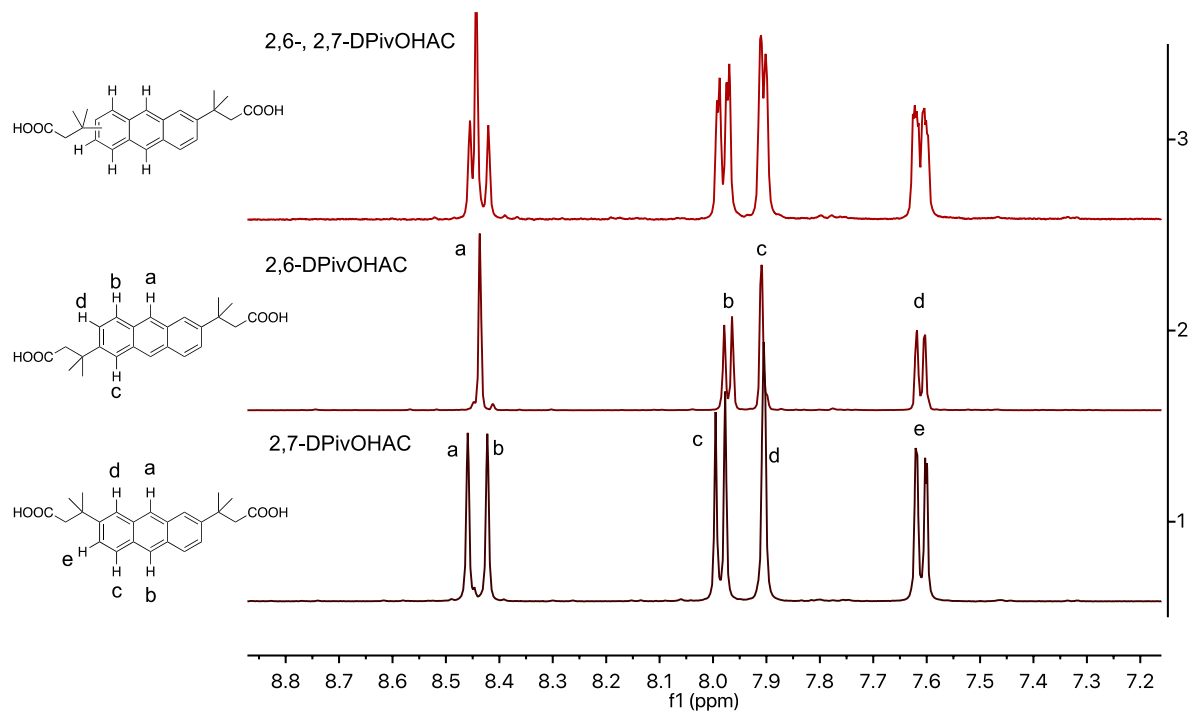
125



126

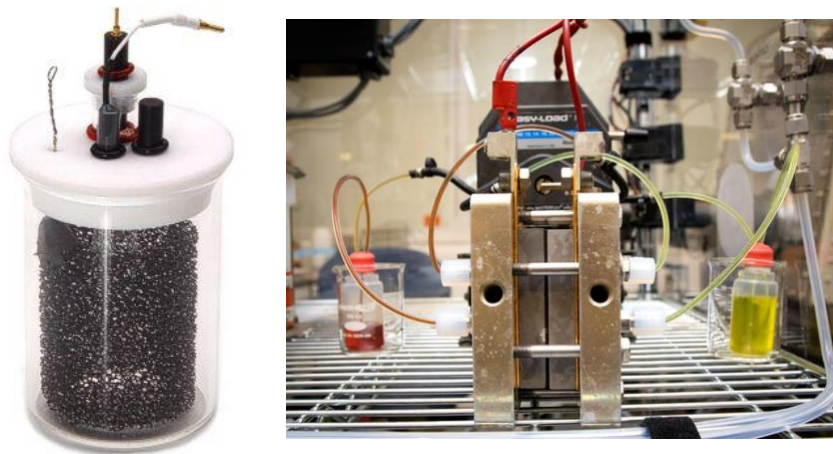
127 **Figure S1.** ¹H NMR spectra of commercial and synthesized 9,10-dihydroanthracene (**DHAC**) in
128 DMSO-*d*₆.

129



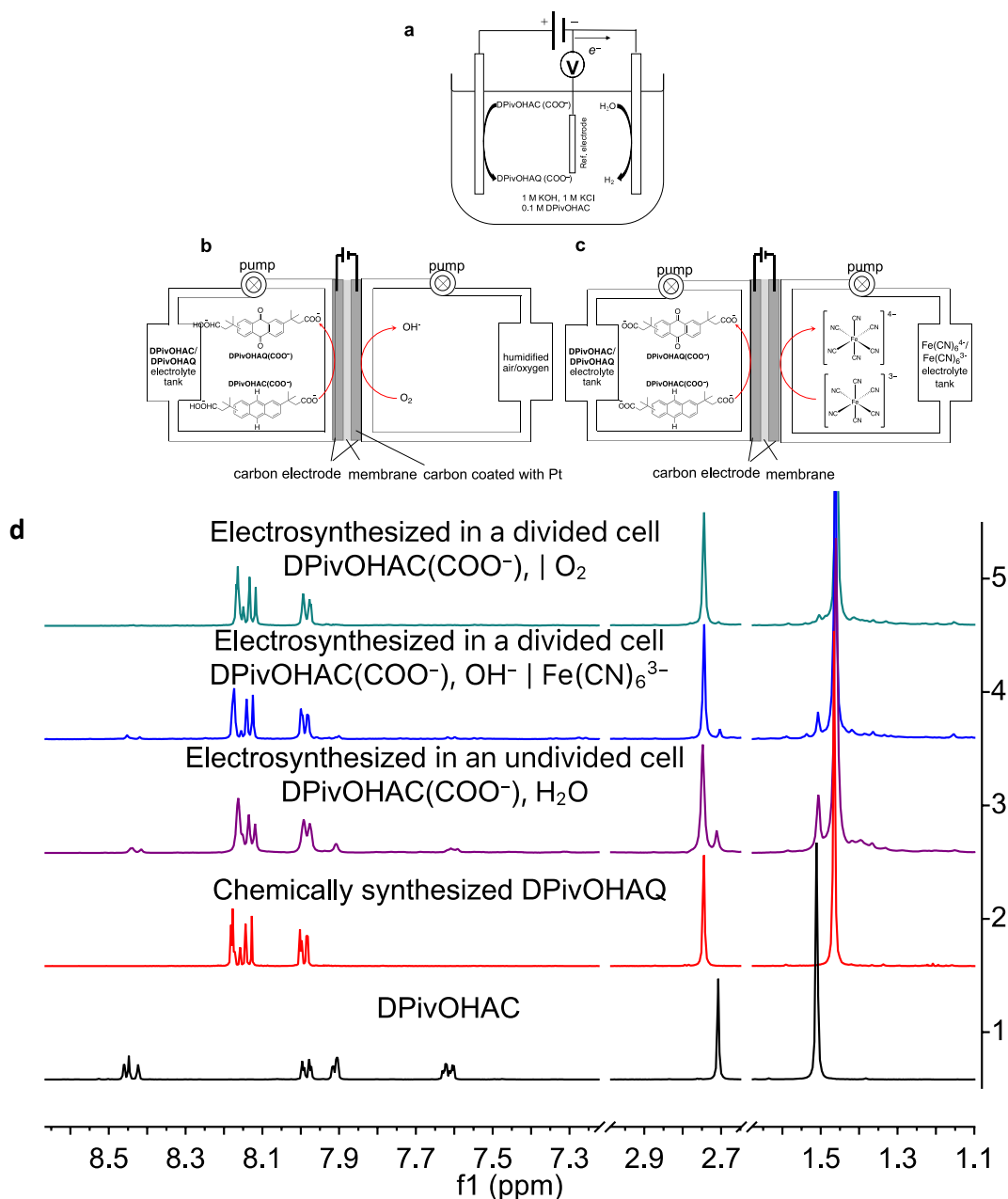
130
 131 **Figure S2.** ^1H NMR spectra of 2,7-, 2,6-DPivOHAC isomers and their mixture (aromatic region)
 132 in $\text{DMSO-}d_6$.
 133

a Undivided cell **b** Divided cell



134
 135 **Figure S3.** Photos of undivided cell (a) and divided cell (b).
 136

137



138

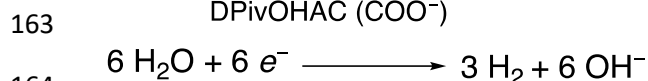
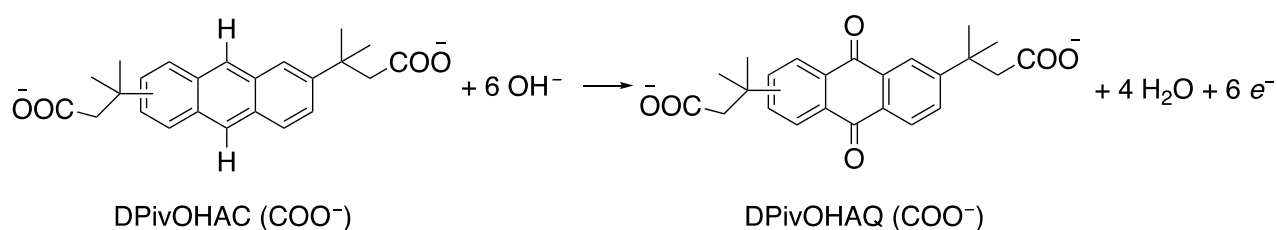
139

140 **Figure S4.** Schematics of (a) undivided cell against the HER and divided cells against (b) the ORR141 and (c) ferricyanide to ferrocyanide, respectively. (d) ¹H NMR spectra of (bottom to top):142 chemically synthesized **DPivOHAC** (black); chemically synthesized **DPivOHAQ** (red);143 electro-synthesized **DPivOHAQ** in an undivided cell (purple), 17.3% of **DPivOHAC** remained144 unreacted according to the integration, yield: 82.7%; electro-synthesized **DPivOHAQ** in a divided145 cell against Fe(CN)₆³⁻ (blue), 7.0% of **DPivOHAC** remained unreacted according to the146 integration, yield: 93.0%; electro-synthesized **DPivOHAQ** in a divided cell against O₂ (green), 0 %147 of **DPivOHAC** remained unreacted according to the integration, yield: 100%. The deuterated148 solvent is DMSO-*d*₆, and the solvent peaks (DMSO and H₂O) were removed to better display the149 peaks of interest. The electrochemical details are described under the headings **Electrosynthesis**150 **I, II, and III.**

150

151 No ion-selective membrane is needed in the undivided cell (against the HER), nor are hydroxides
 152 required theoretically because the HER generates the required number of hydroxides for
 153 **DPivOHAQ** electrosynthesis. Ideally, the divided cell against the ORR will not require hydroxides
 154 either if all generated hydroxides from the ORR can immediately crossover to the **DPivOHAC**
 155 anolyte side. The divided cell against ferri- to ferrocyanide reduction needs six equivalents of
 156 hydroxide for electrosynthesis, the advantage of which is incorporating the electrosynthesis and
 157 flow battery in one setup, and electrosynthesis becomes a part of the on-site setup and takes as
 158 long as the energy/power ratio of the battery.

159
 160 **Electrosynthesis I.** Electrochemical synthesis of **DPivOHAQ(COO⁻)** in an undivided cell at 0.1
 161 M concentration, against the hydrogen evolution reaction (HER).
 162



165
 166 An undivided cell was prepared with carbon felt (XF30A, Toyobo Co., volumetric porosity: 95%)
 167 as the working electrode, a carbon rod as the counter electrode, and Ag/AgCl (3 M NaCl) as the
 168 reference electrode.

169
 170 Electrolyte preparation: 0.378 g **DPivOHAC**, 0.745 g KCl, and 0.561 g KOH were dissolved in
 171 deionized water to obtain a 10 mL solution containing 0.1 M **DPivOHAC**, 1.0 M KCl, and 1.0 M
 172 KOH.

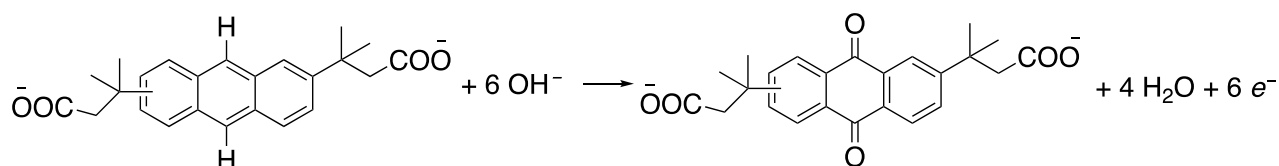
173
 174 On the working electrode: **DPivOHAC(COO⁻)** was oxidized to **DPivOHAQ(COO⁻)**; on the
 175 counter electrode: water was reduced to hydrogen gas.

176
 177 Electrochemical oxidation of **DPivOHAC(COO⁻)**: while the electrolyte was stirred, a constant
 178 potential (1.1 V vs. Ag/AgCl) was applied to the divided electrolytic cell until 120% of the required
 179 coulombs were extracted from the working electrode. [0.1 M * 0.01 L * 96485 C/mol * 6 * 1.2 =
 180 694.7 C, 6 electrons need to be extracted from every **DPivOHAC** molecule].

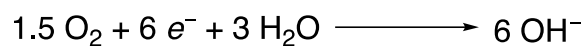
181
 182 Characterization of anolyte: an aliquot (~250 μL) was transferred from the as-prepared anolyte to
 183 an Eppendorf® tube (capacity: 1.5 mL) and acidified by a drop of concentrated HCl to obtain
 184 **DPivOHAQ** precipitate. The final **DPivOHAQ** precipitate was re-dissolved in DMSO-*d*₆ for ¹H
 185 NMR measurement. According to the integration of the ¹H NMR spectrum (Figure 3d), the yield
 186 is 82.7%. The faradaic efficiency (%) = [yield (%) / 1.2] = 68.9%.

187
 188

189 **Electrosynthesis II.** Electrochemical synthesis of **DPivOHAQ(COO⁻)** in a divided cell at 0.1 M
 190 concentration, against the oxygen reduction reaction (ORR).
 191



192



193

194

195 In a flow cell setup (divided electrolytic cell), where unbaked AvCarb HCBA was used on the
 196 anode side, carbon paper was used on the cathode side with coated platinum particles to catalyze
 197 the ORR; Nafion® 212 was used as the membrane. The high-frequency area specific resistance
 198 (HF-ASR) was maintained in the range of 1.48–1.54 Ω cm² before and after electrosynthesis.
 199

199

200 Anolyte preparation: 0.378 g **DPivOHAC**, 0.745 g KCl, and 0.561 g KOH were dissolved in
 201 deionized water to obtain a 10 mL solution containing 0.1 M **DPivOHAC**, 1.0 M KCl, and 1.0 M
 202 KOH.
 203

203

204 Catholyte preparation: humidified oxygen or air was pumped into the flow cell to participate in
 205 the electrochemical reaction.
 206

206

207 Electrochemical oxidation of **DPivOHAC(COO⁻)**: a constant voltage (1.8 V) was applied to the
 208 divided electrolytic cell until the current decreased to 2 mA/cm². The number of extracted electrons
 209 was ~1.2 times higher than the theoretical value.
 210

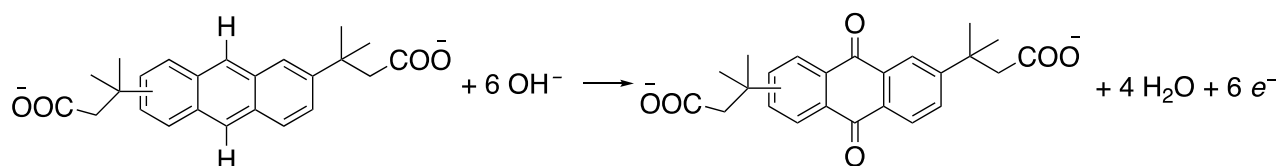
210

211 Characterization of anolyte: an aliquot (~250 μL) was transferred from the as-prepared anolyte to
 212 an Eppendorf® tube (capacity: 1.5 mL) and acidified by concentrated HCl to obtain **DPivOHAQ**
 213 precipitate. The final **DPivOHAQ** precipitate was re-dissolved in DMSO-*d*₆ for ¹H NMR
 214 measurement. According to the integration of the ¹H NMR spectrum (Figure 3d), the yield is 100%.
 215 The faradaic efficiency (%) = [yield (%) / 1.2] = 83.3%.
 216

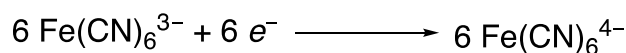
216

217 **Electrosynthesis III.** Electrochemical synthesis of **DPivOHAQ(COO⁻)** in a divided cell at 0.1 M
 218 concentration, against the reduction of ferricyanide.
 219

219



220



221

222

223 In a flow cell setup (divided electrolytic cell), unbaked AvCarb HCBA (woven carbon cloth) was
 224 used as electrodes for both sides; Nafion® 212 was used as the membrane. The high-frequency

225 area specific resistance (HF-ASR) was maintained at $\sim 1.12 \Omega \text{ cm}^2$ before and after
226 electrosynthesis.

227
228 Anolyte preparation: 0.378 g **DPivOHAC**, 0.745 g KCl, and 0.561 g KOH were dissolved in
229 deionized water to obtain a 10 mL solution containing 0.1 M **DPivOHAC**, 1.0 M KCl, and 1.0 M
230 KOH.

231
232 Catholyte preparation: 3.292 g $\text{K}_3\text{Fe}(\text{CN})_6$, 7.445 g KCl, and 2.805 g KOH were dissolved in
233 deionized water to obtain a 100 mL solution containing 0.1 M $\text{K}_3\text{Fe}(\text{CN})_6$, 1.0 M KCl, and 0.5 M
234 KOH.

235
236 The reason for which 0.5 M KOH was added to the catholyte is to counterbalance the added OH^- in
237 the anolyte, which is required for the electrosynthesis, thereby suppressing the loss of OH^- from
238 the anolyte to the catholyte due to crossover.

239
240 Electrochemical oxidation of **DPivOHAC(COO⁻)**: a constant current density (20 mA/cm²) was
241 applied to the divided cell for at most 1.5 hours with a 1.2 V voltage cutoff; when either time or
242 voltage reached the limit, the potential was held (1.2 V vs. ferro-/ferricyanide) until the current
243 decreased to 2 mA/cm². The number of extracted electrons was ~ 1.2 times higher than the
244 theoretical value.

245
246 Characterization of anolyte: an aliquot ($\sim 250 \mu\text{L}$) was transferred from the as-prepared anolyte to
247 an Eppendorf® tube (capacity: 1.5 mL) and acidified by a drop of concentrated HCl to obtain
248 **DPivOHAQ** precipitate. The final **DPivOHAQ** precipitate was re-dissolved in DMSO-*d*₆ for ¹H
249 NMR measurement. According to the integration of the ¹H NMR spectrum (Figure 3d), the yield
250 is 93.0%. The faradaic efficiency (%) = [yield (%) / 1.2] = 77.5%.

251
252 Because a few aliquots were transferred and the volume of as-prepared **DPivOHAQ** changed, 5
253 mL of the **DPivOHAQ** solution was used as the negolyte and 100 mL of the ferro-/ferricyanide
254 solution [$\sim 0.06 \text{ M K}_4\text{Fe}(\text{CN})_6$ and $\sim 0.04 \text{ M K}_3\text{Fe}(\text{CN})_6$] generated from **Electrosynthesis III** was
255 used as the posolyte for charge-discharge cycling. Due to leakage, 4.5 mL of **DPivOHAQ**
256 remained for subsequent cycling.

257
258 **Electrosynthesis IV.** Electrochemical synthesis of **DPivOHAQ(COO⁻)** in a divided cell at 0.5 M
259 concentration with excess hydroxide, against the reduction of ferricyanide.

260
261 In a flow cell setup (divided electrolytic cell), unbaked AvCarb HCBA (woven carbon cloth) was
262 used as electrodes for both sides; Nafion® 212 was used as the membrane. The high-frequency
263 area specific resistance (HF-ASR) was maintained at $\sim 1.1 \Omega \text{ cm}^2$ before and after electrosynthesis.

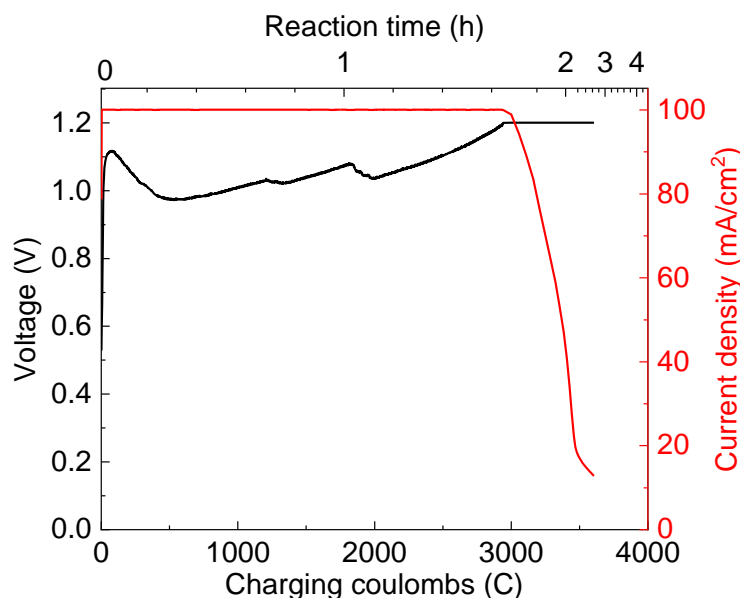
264
265 Anolyte preparation: 1.89 g **DPivOHAC**, 0.745 g KCl, and 0.567 g KOH were dissolved in
266 deionized water to obtain a 10 mL solution containing 0.5 M **DPivOHAC**, 1.0 M KCl, and 1.0 M
267 KOH. Although the **DPivOHAC** electrochemical oxidation requires OH^- ions, we observed that
268 0.5 M **DPivOHAC** tends to crash out of solution when the concentration of KOH exceeds 1.5 M.
269 To circumvent this precipitation issue, we added 1.5 times the required amount of KOH pellets

270 (2.52 g) (*i.e.*, 1.5 times 6 equivalents relative to **DPivOHAC**) into the analyte over the course of
271 constant current charging. According to the Nernst equation, the cell voltage is a function of [OH⁻];
272 thus, the voltage fluctuation reflects the addition of KOH in Figure S5.

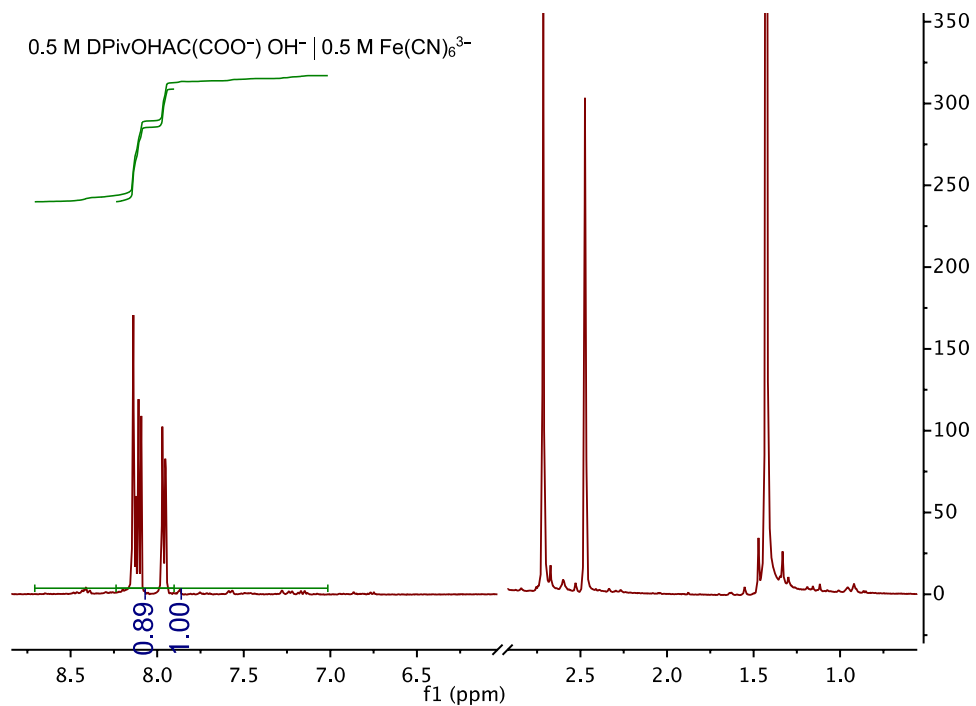
273
274 Catholyte preparation: 16.46 g K₃Fe(CN)₆, 7.445 g KCl, and 2.805 g KOH were dissolved in
275 deionized water to obtain a 100 mL solution containing 0.5 M K₃Fe(CN)₆, 1.0 M KCl, and 0.5 M
276 KOH.

277
278 Electrochemical oxidation of **DPivOHAC(COO⁻)**: a constant current density (100 mA/cm²) was
279 applied to the divided cell for at most 1.7 hours with a 1.2 V voltage cutoff; when either time or
280 voltage reached the limit, the potential was held (1.2 V vs. ferro-/ferricyanide) until the current
281 decreased to 12 mA/cm². The number of extracted electrons was ~1.2 times higher than the
282 theoretical value.

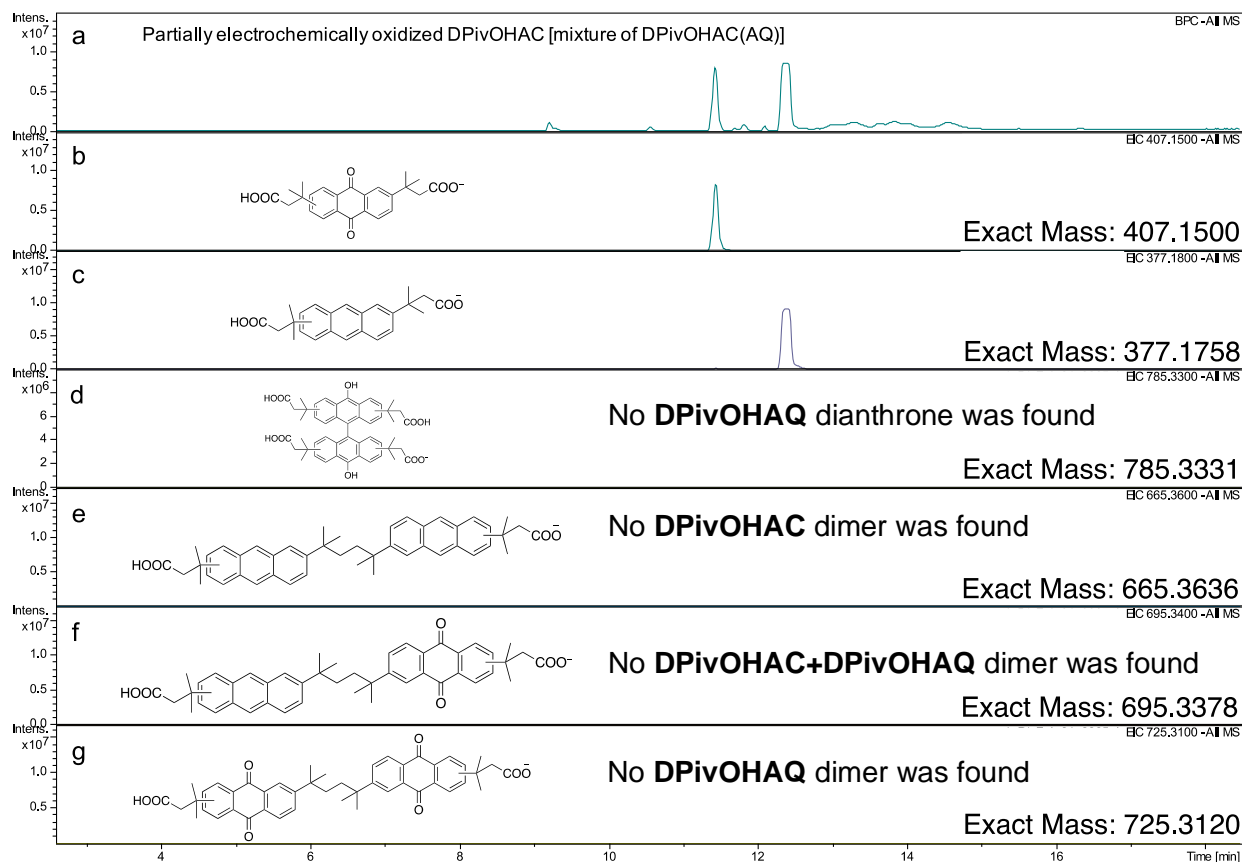
283
284 Characterization of analyte: an aliquot (~250 μL) was transferred from the as-prepared analyte to
285 an Eppendorf® tube (capacity: 1.5 mL) and acidified by a drop of concentrated HCl to obtain
286 **DPivOHAQ** precipitate. The final **DPivOHAQ** precipitate was re-dissolved in DMSO-*d*₆ for ¹H
287 NMR measurement; the yield is 89.0%. The faradaic efficiency (%) = [yield (%) / 1.2] = 74.2%.



288
289 **Figure S5.** The electrochemical oxidation of 0.5 M **DPivOHAC(COO⁻)** (**Electrosynthesis IV**).

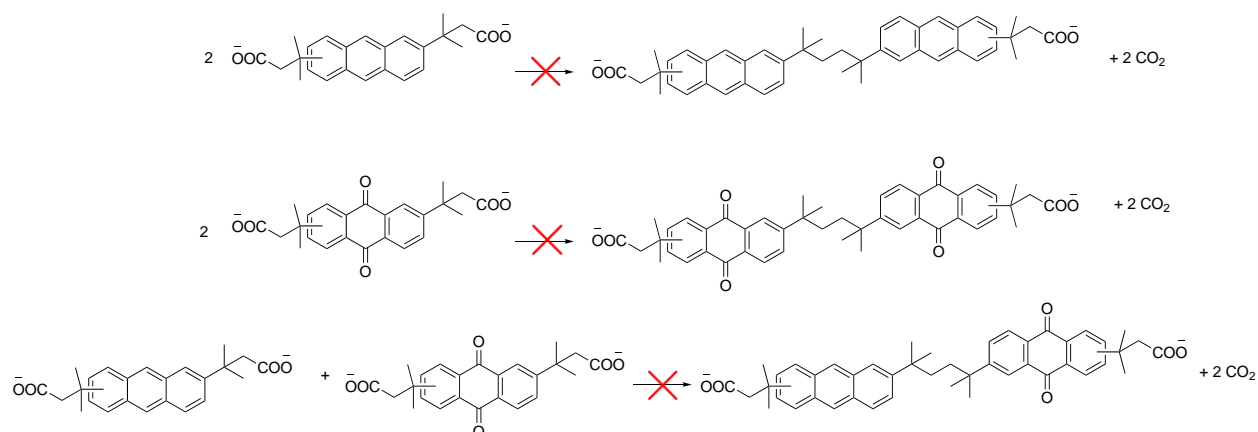


290
 291 **Figure S6.** ¹H NMR spectrum of **DPivOHAQ** in DMSO-*d*₆ synthesized via the procedure
 292 described in **Electrosynthesis IV**. From the aromatic peak integrations, we found that 89.0%
 293 **DPivOHAQ** was generated (when the two sets of peaks at chemical shifts of 7.95 and 8.10 ppm
 294 were integrated), 11.0% **DPivOHAC** was remaining.
 295



296
 297 **Figure S7.** Mass spectra of partially electrochemically oxidized **DPivOHAQ** (from **Electrosynthesis IV**)
 298 measured by liquid chromatography–mass spectrometry (LC–MS). (a) The peak intensity and
 299 retention time of partially electrochemically oxidized **DPivOHAQ** under negative mode. (b) The peak
 300 intensity and retention time of **DPivOHAQ** under negative mode. (c) The peak intensity and
 301 retention time of **DPivOHAC** under negative mode. (d) The peak intensity and retention time of
 302 the **DPivOHAQ** dianthrone under negative mode. No peak was found in the given retention time
 303 region, which, in combination with the absence of impurities in the ^1H NMR spectra in Figures 3d
 304 and S6, indicates that no observable **DPivOHAQ** dianthrone was generated during the
 305 electrochemistry. (e)–(g) The peak intensity and retention time of **DPivOHAQ(AC)**-related Kolbe
 306 electrolysis byproducts under negative mode. No peak was found in the given retention time region,
 307 which, in combination with the absence of impurities in the ^1H NMR spectra in Figures 3d and S6,
 308 indicates that no observable **DPivOHAQ(AC)**-related Kolbe electrolysis byproducts were
 309 generated during the electrochemistry.

NO Kolbe electrolysis



310 **Scheme S1.** Kolbe electrolysis. Kolbe electrolysis-related byproducts are not expected in our cell,
311 as the decarboxylation and dimerization reactions usually require much higher voltages and
312 precious-metal-based electrodes.^{s1} In our cell, we use carbon electrodes and an applied potential
313 of 1.2 V. Additionally, we did not detect any dimer formation from LC–MS measurements.

314
315 **Electrosynthesis V.** Electrochemical synthesis of **DPivOHAQ(COO⁻)** in a divided cell at 0.5 M
316 concentration with a stoichiometric quantity of hydroxide, against the reduction of ferricyanide.

317
318 In a flow cell setup (divided electrolytic cell), unbaked AvCarb HCBA (woven carbon cloth) was
319 used as electrodes for both sides; Nafion® 212 was used as the membrane. The high-frequency
320 area specific resistance (HF–ASR) was maintained at $\sim 1.45 \Omega \text{ cm}^2$ before and after
321 electro-synthesis.

322
323 Anolyte preparation: 1.89 g **DPivOHAC**, 0.745 g KCl, and 0.567 g KOH were dissolved in
324 deionized water to obtain a 10 mL solution containing 0.5 M **DPivOHAC**, 1.0 M KCl, and 1.01
325 M KOH. We added the stoichiometric quantity of KOH pellets (1.68 g) (*i.e.*, 6 equivalents relative
326 to **DPivOHAC**) into the anolyte over the course of constant current charging.

327
328 Catholyte preparation: 16.46 g $\text{K}_3\text{Fe}(\text{CN})_6$, 7.445 g KCl, and 2.805 g KOH were dissolved in
329 deionized water to obtain a 100 mL solution containing 0.5 M $\text{K}_3\text{Fe}(\text{CN})_6$, 1.0 M KCl, and 0.5 M
330 KOH.

331
332 Electrochemical oxidation of **DPivOHAC(COO⁻)**: a constant current density (100 mA/cm²) was
333 applied to the divided electrolytic cell for at most 1.7 hours with a 1.2 V voltage cutoff; when
334 either time or voltage reached the limit, the potential was held (1.2 V vs. ferro-/ferricyanide) until
335 the current decreased to 12 mA/cm². The number of extracted electrons was ~ 1.2 times higher than
336 the theoretical value.

337
338 Characterization of anolyte: an aliquot ($\sim 250 \mu\text{L}$) was transferred from the as-prepared anolyte to
339 an Eppendorf® tube (capacity: 1.5 mL) and acidified by a drop of concentrated HCl to obtain
340 **DPivOHAQ** precipitate. The final **DPivOHAQ** precipitate was re-dissolved in DMSO-*d*₆ for ¹H
341 NMR measurement; the yield is 81.8%. The faradaic efficiency (%) = [yield (%) / 1.2] = 68.2%.

342
343

344 **Formation of dianthrone during electrosynthesis**

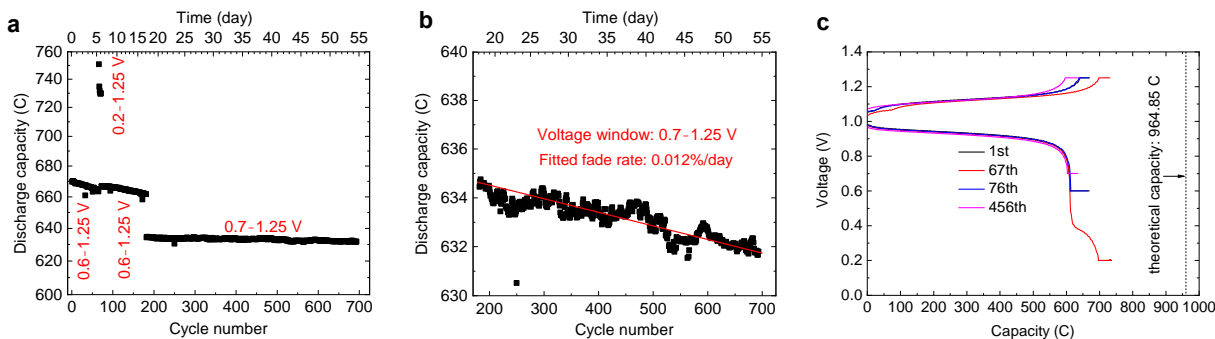
345 Anthrone dimers can be produced during the electrosynthesis when insufficient hydroxide is
346 present.

347
348 When there is excess hydroxide in the solution, although some OH⁻ ions will be electrochemically
349 oxidized to oxygen via the OER, the remaining OH⁻ ions are sufficient for the conversion of A⁻ to
350 AQ₂⁻.

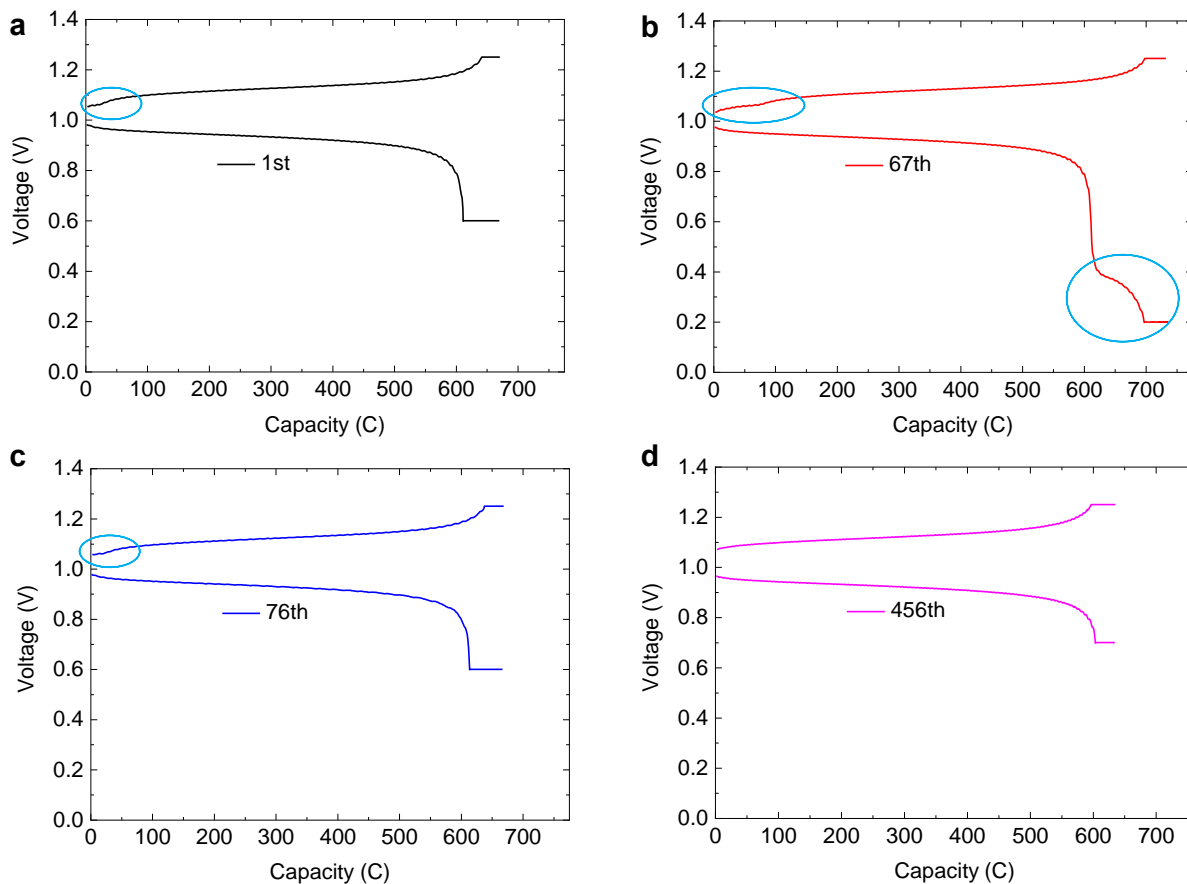
351
352 When there is no excess hydroxide, given that the OER side reaction is an inevitable competing
353 reaction, there will be insufficient OH⁻ ions for the conversion of A⁻ to AQ₂⁻; instead, the
354 anthrone anion A⁻ may be oxidatively dimerized to the dianthrone DA. The following figures and
355 scheme illustrate how DA was identified and propose its corresponding electrochemistry.

356
357 During the electrochemical oxidation of the 10 mL 0.5 M DPivOHAC(COO⁻) at pH 12, only 1.68
358 g of KOH (10*0.001 L*0.5 M*6*56.1056 g/mol = 1.68 g) were added to the solution. Although
359 there is some additional KOH added to the potassium ferricyanide side, hydroxide cannot cross
360 over to the DPivOHAC side of the cell sufficiently rapidly to offset its consumption by
361 DPivOHAC oxidation and the OER.

362

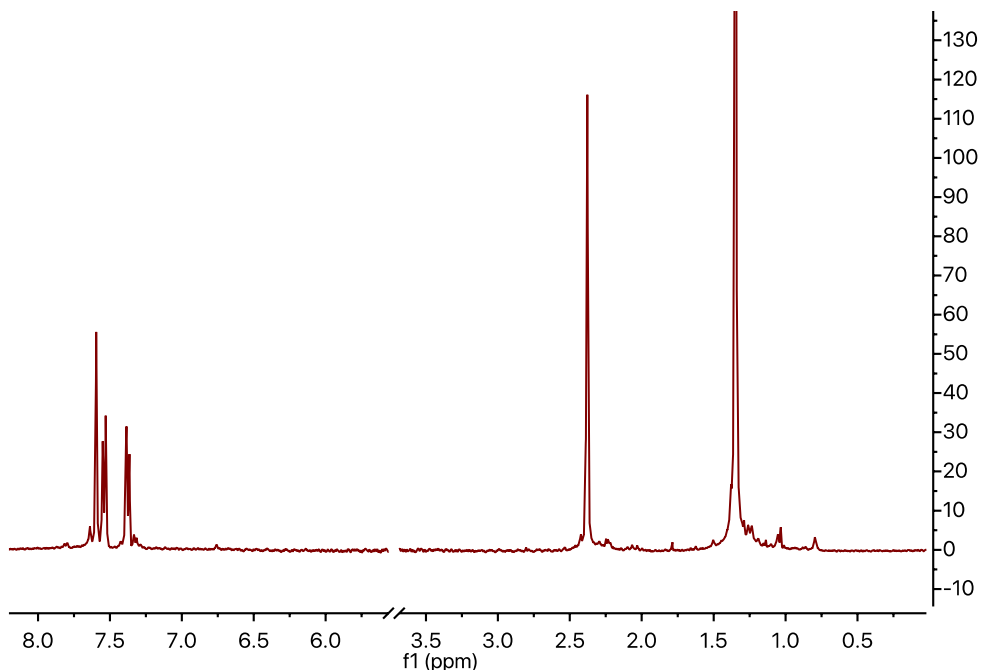


363
364 **Figure S8.** Cell performance of 0.5 M electrosynthesized DPivOHAQ when a stoichiometric
365 quantity of hydroxide was added into the DPivOHAC(COO⁻) solution (**Electrosynthesis V**). (a)
366 The long-term cycling performance with adjusted lower voltage cutoffs. (b) The zoomed in
367 discharge capacity when 0.7–1.25 V voltage cutoffs were applied; the fitted temporal fade rate
368 was 0.01%/day. (c) The voltage profiles at varying cycle numbers with different lower voltage
369 cutoffs.



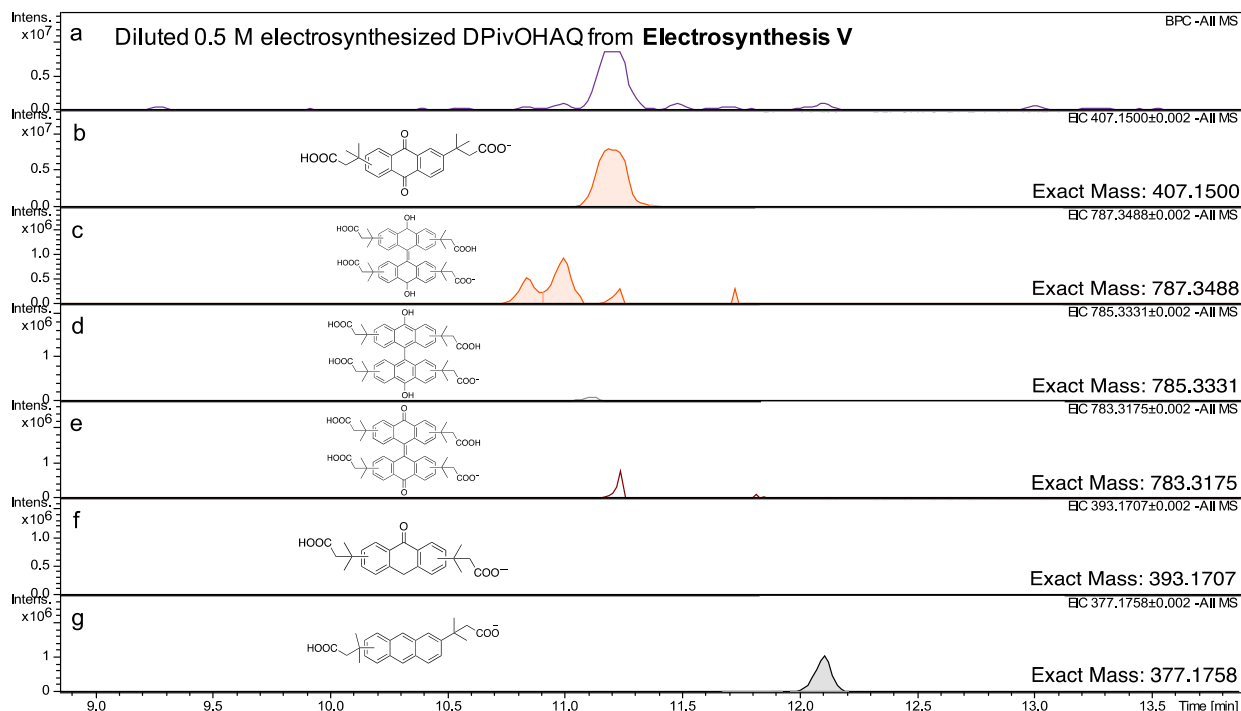
370
 371 **Figure S9.** Voltage profiles of 0.5 M electrosynthesized **DPivOHAQ** when a stoichiometric
 372 quantity of hydroxide was added into the **DPivOHAC** solution (**Electrosynthesis V**) with
 373 different lower voltage cutoffs [(a) 0.6, (b) 0.2, (c) 0.6, and (d) 0.7 V]. The upper voltage cutoff is
 374 kept constant at 1.25 V for the duration of cell cycling.

375
 376 In the 1st cycle, the region in (a) circled in cyan shows a small plateau, indicating some redox-
 377 active byproducts were produced during the electrosynthesis. In the 67th cycle, after lowering the
 378 lower cutoff from 0.6 to 0.2 V, we can clearly see the discharge plateau (in the region of 0.2–0.4
 379 V) attributed to byproducts, and the charge plateau attributed to byproducts is also becoming
 380 longer. In the 76th cycle, after elevating the lower cutoff back to 0.6 V, the shape of the charge
 381 profile becomes nearly the same as the one in the 1st cycle. After the lower voltage cutoff was
 382 further increased to 0.7 V, in the 456th cycle, the small plateau attributed to the byproducts
 383 disappeared.

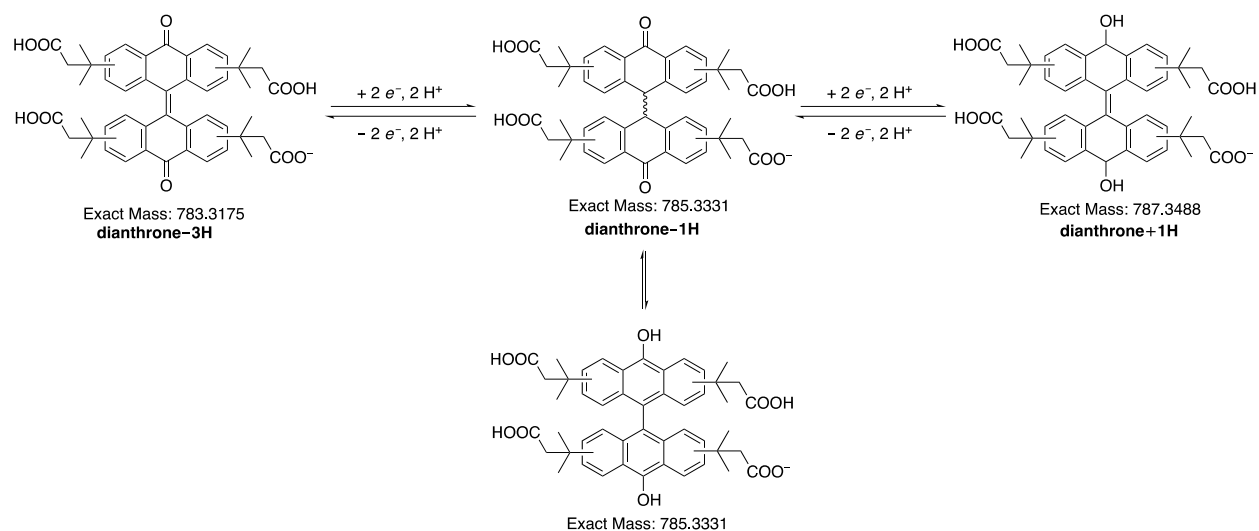


384
 385 **Figure S10.** ^1H NMR spectrum of cycled 0.5 M electrosynthesized **DPivOHAQ** when a
 386 stoichiometric quantity of hydroxide was added into the **DPivOHAC(COO⁻)** solution
 387 (**Electrosynthesis V**). The solvent peak was removed to clearly show both aromatic and aliphatic
 388 regions of the cycled **DPivOHAQ** solution. The deuterated solvent is D_2O . The dominant peaks
 389 can be assigned to **DPivOHAQ**. Some small impurity peaks were observed, but they are difficult
 390 to identify. The percentages of side products are very close to the detection limit of the ^1H NMR
 391 instrument.

392
 393
 394

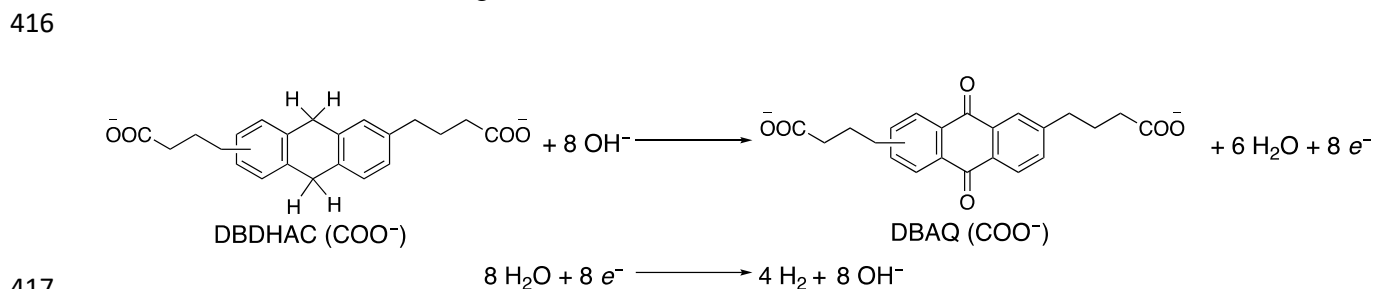


395
 396 **Figure S11.** LC-MS results of cycled 0.5 M electrosynthesized **DPivOHAQ** when a
 397 stoichiometric quantity of hydroxide was added into the **DPivOHAC** solution (**Electrosynthesis**
 398 **V**). (a) The base peak chromatogram of the sample, showing all peaks observed by mass
 399 spectrometry under negative mode. (b) The peak intensity and retention time of **DPivOHAQ-1H**
 400 under negative mode. (c) The peak intensity and retention time of **dianthrone+1H** under negative
 401 mode. (d) The peak intensity and retention time of **dianthrone-1H** under negative mode. (e) The
 402 peak intensity and retention time of **dianthrone-3H** under negative mode. (f) The peak intensity
 403 and retention time of **anthrone-1H** under negative mode (none observed). (g) The peak intensity
 404 and retention time of **DPivOHAC-1H** under negative mode. By integrating the peak areas in (b),
 405 (c), (d), (e), (f) and (g), we found the percentages of **DPivOHAQ** (81.8%), **dianthrone+1H**
 406 (10.2%), **dianthrone-1H** (0.4%), **dianthrone-3H** (1.3%), and **DPivOHAC** (6.3%).
 407



408
409 **Scheme S2.** Proposed possible redox reactions of dianthrones. Because the **dianthrono+1H** (exact
410 mass: 787.3488) and **dianthrono-3H** (exact mass: 783.3175) were detected and plateaus were
411 observed from the voltage profiles, we propose that there are three redox-active states for the
412 dianthrones.

413
414 **Electrosynthesis VI.** Electrochemical synthesis of **DBAQ(COO⁻)** in an undivided electrolytic
415 cell at 0.1 M concentration, against the HER.



417
418 An undivided electrolytic cell was prepared with carbon felt (XF30A, Toyobo Co., volumetric
419 porosity: 95%) as the working electrode, a carbon rod as the counter electrode, and Ag/AgCl (3 M
420 NaCl) as the reference electrode.

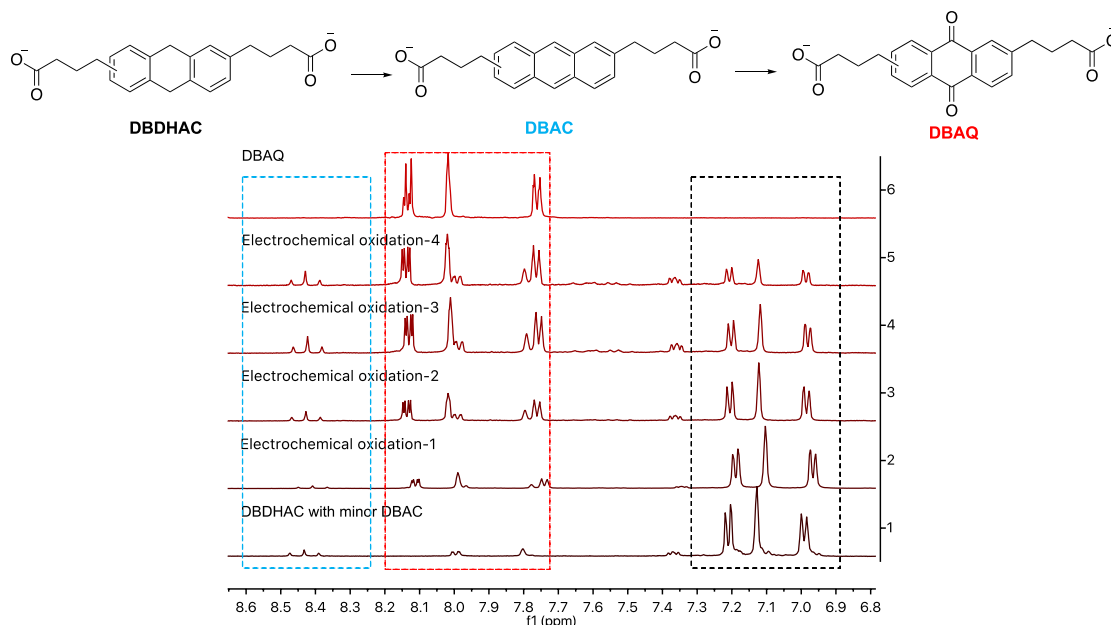
421
422 Electrolyte preparation: 0.35 g **DBDHAC**, 0.745 g KCl, and 0.561 g KOH were dissolved in
423 deionized water to obtain a 10 mL solution containing 0.1 M **DBDHAC**, 1.0 M KCl, and 1.0 M
424 KOH.

425
426 On the working electrode: **DBDHAC** was oxidized to **DBAQ**; on the counter electrode: water was
427 reduced to hydrogen gas.

428
429 Electrochemical oxidation of **DBDHAC(COO⁻)**: while the electrolyte was stirring, a constant
430 potential (1.1 V vs. Ag/AgCl) was applied to the divided electrolytic cell until 120% of the required
431 coulombs were extracted from the working electrode. [0.1 M * 0.01 L * 96485 C/mol * 8 * 1.2 =
432 926.3 C; 8 electrons need to be extracted from every **DBDHAC** molecule].

434

435 Characterization of analyte: an aliquot (250 μL) was transferred from the as-prepared analyte to
 436 an Eppendorf® tube (capacity: 1.5 mL) and acidified by a drop of concentrated HCl to obtain
 437 **DBAQ** precipitate. The final **DBAQ** precipitate was re-dissolved in $\text{DMSO-}d_6$ for ^1H NMR
 438 measurement. According to the integration of the ^1H NMR spectrum in the Figure S12, the yield
 439 is 70%. The faradaic efficiency (%) = [yield (%) / 1.2] = 58.3%.
 440



441 **Figure S12.** ^1H NMR spectra of **DBDHAC** (bottom), chemically synthesized **DBAQ** (top), and
 442 electrochemically synthesized **DBAQ** in an undivided cell after varying extents of reaction.
 443 **DBDHAC**: 4,4'-(9,10-dihydroanthracene-diyl)dibutanoic acid; **DBAC**: 4,4'-(anthracene-
 444 diyl)dibutanoic acid; **DBAQ**: 4,4'-(9,10-anthraquinone-diyl)dibutanoic acid. The time interval
 445 between successive measurements labeled electrochemical oxidation-1, 2, 3, and 4 is
 446 approximately one hour. The deuterated solvent is $\text{DMSO-}d_6$.
 447
 448

449 Light sensitivity experiments

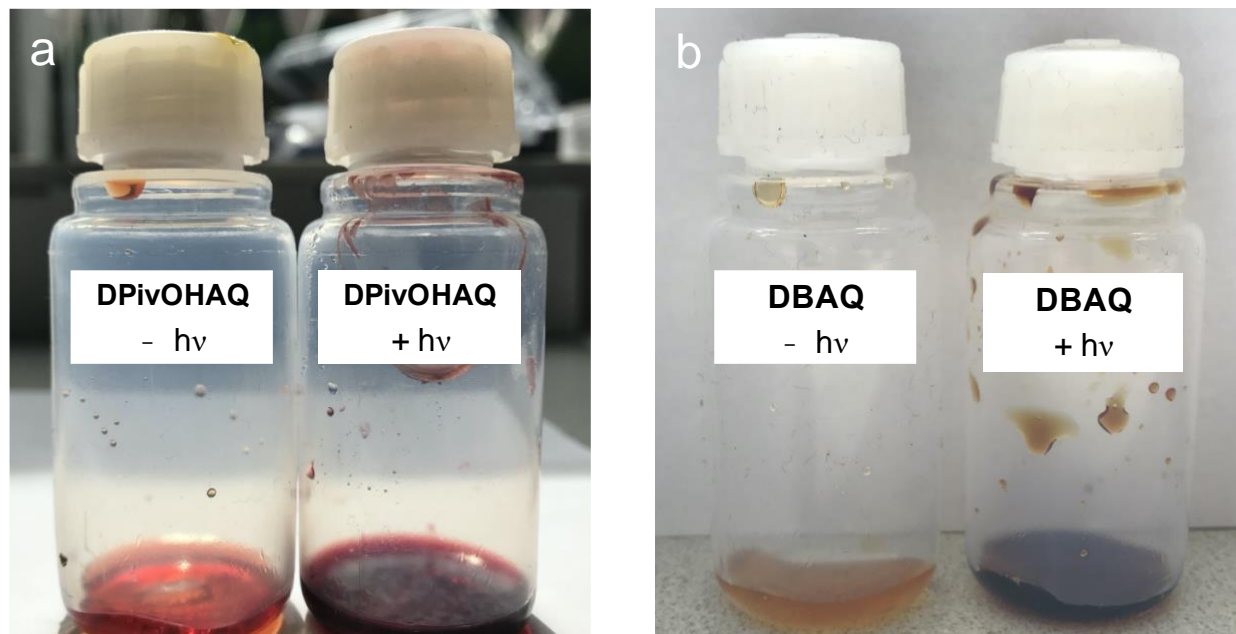
450 It has been reported that quinones and related compounds can decompose in the presence of
 451 light.^{s3-s7} In order to determine the light sensitivity of **DPIvOHAQ** and **DBAQ**, we compared
 452 solutions of each compound held in the presence of and in the absence of light for 1 week. Two
 453 samples of **DPIvOHAQ** (0.1 M, pH 12 in water with 1 M KCl, 1.5 mL each) and two samples of
 454 **DBAQ** (0.1 M, pH 12 in water, 1.5 mL each) were prepared in separate FEP bottles (VWR Catalog
 455 No. 16071-008). For each compound, one sample was wrapped in aluminum foil and stored in a
 456 dark drawer for 1 week. The other sample was held for 1 week under a quartz halogen lamp with
 457 a controllable output of 50–1000 W set to 500 W (CowboyStudio QL-1000 W HEAD; ePhotoInc
 458 QL 1000Bulb). The samples exposed to light were allowed to float at the top of a water bath
 459 containing approximately 16 L of water to dissipate excess heat produced by the lamp (the liquid
 460 level decreased gradually due to evaporation and was replenished daily). The liquid level was
 461 maintained at a distance of approximately 20 cm from the light source.
 462

463 After 1 week, differences in color were observed between the samples of each compound stored
 464 in the dark and exposed to light (Figure S13). The formation of a film was also observed in the

465 **DPivOHAQ** sample exposed to light. ^1H NMR spectra of each sample demonstrate decomposition
466 of both compounds stored in the presence of light (Figures S14 and S15).

467
468 We therefore wrapped the electrolyte reservoirs with aluminum foil to avoid decomposition due
469 to light exposure during cell cycling.

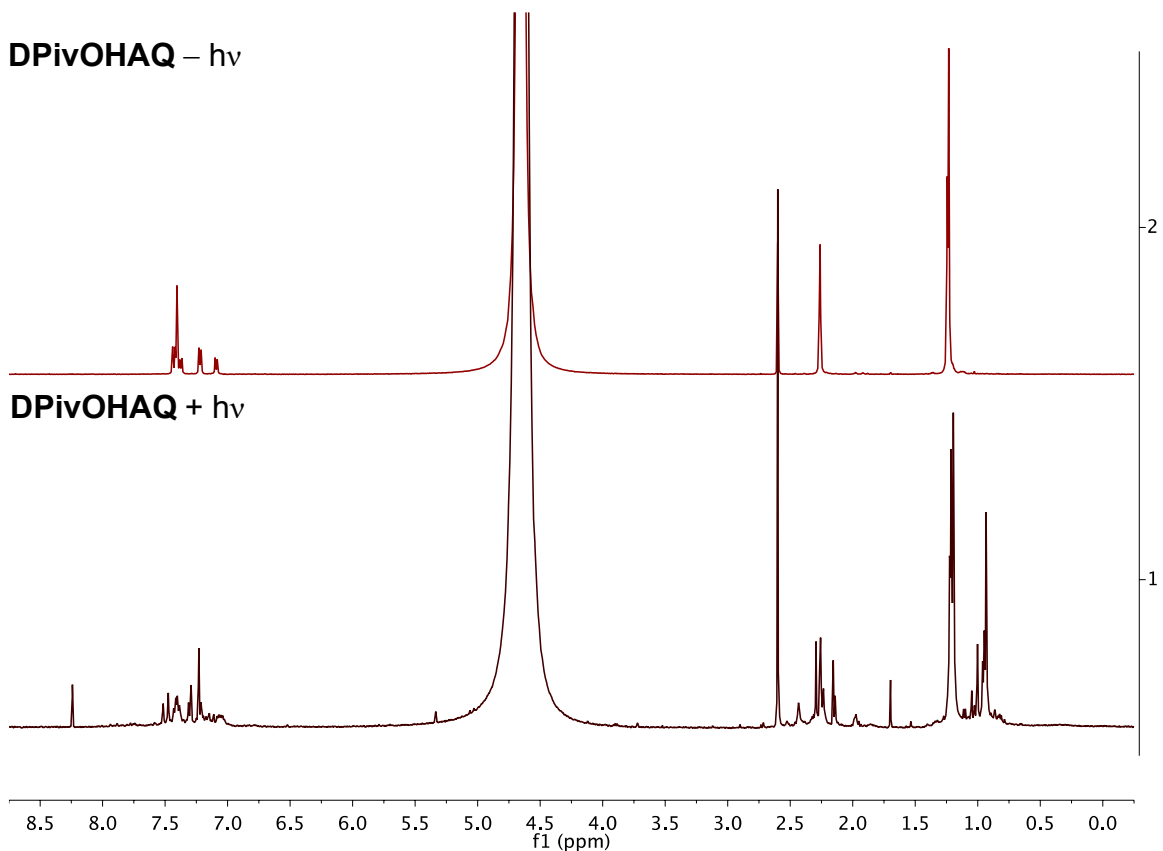
470



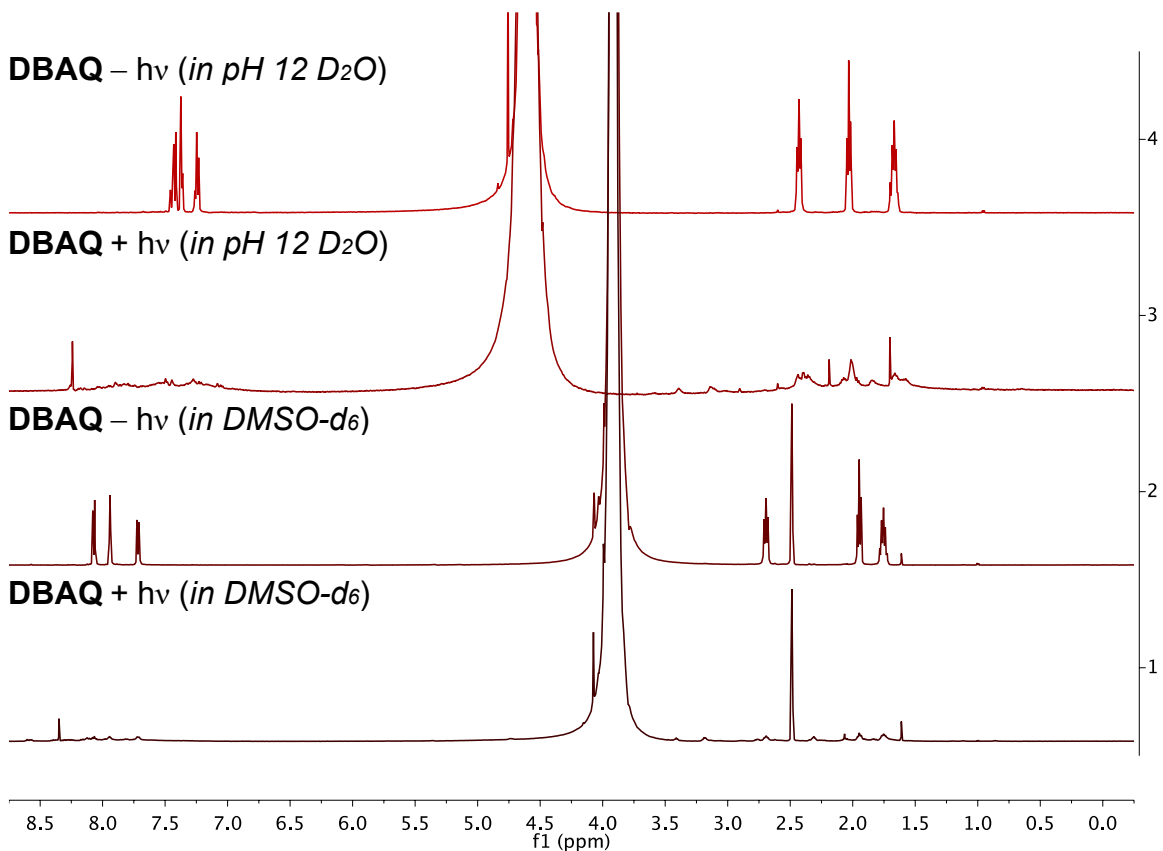
471
472

473 **Figure S13.** Samples of (a) **DPivOHAQ** (0.1 M, pH 12) stored for 1 week in the absence of light
474 ($-h\nu$) and under a 500 W lamp ($+h\nu$) and of (b) **DBAQ** (0.1 M, pH 12) stored for 1 week in the
475 absence of light ($-h\nu$) and under a 500 W lamp ($+h\nu$). Differences in color were observed between
476 the two samples of each compound. The formation of a film was also observed in the **DPivOHAQ**
477 sample exposed to light.

478



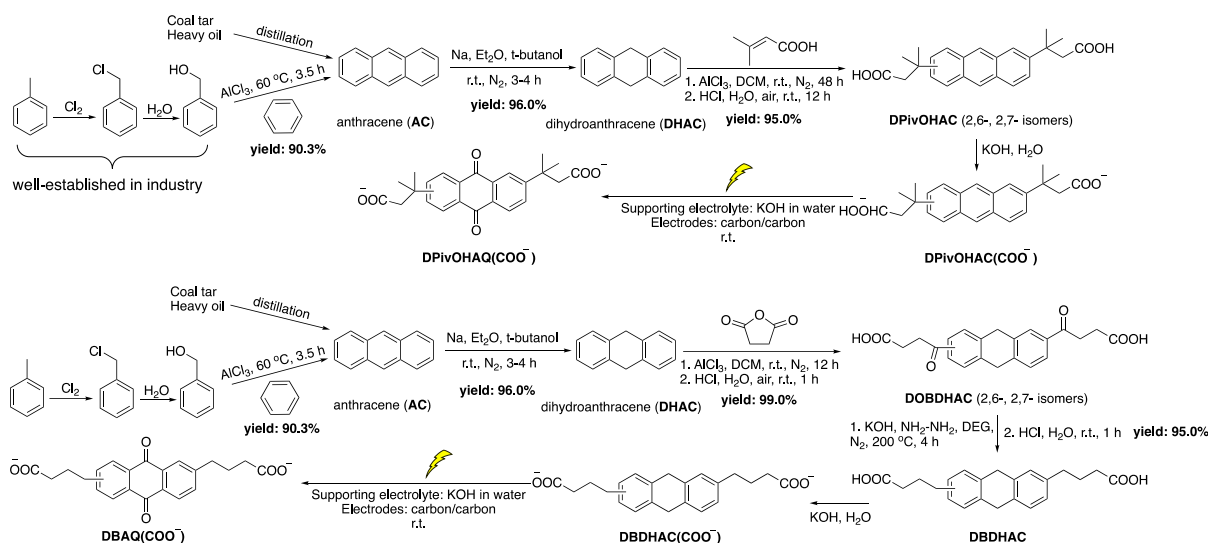
479
 480 **Figure S14.** ^1H NMR spectra of samples of **DPivOHAQ** (0.1 M, pH 12) stored for 1 week in the
 481 absence of light ($-h\nu$) and under a 500 W lamp ($+h\nu$), each diluted (1:5.5) in pH 14 D_2O (1 M
 482 KOD) containing a 9 mM NaCH_3SO_3 internal standard (δ 2.6 ppm).



483
 484 **Figure S15.** ¹H NMR spectra of samples of **DBAQ** (0.1 M, pH 12) stored for 1 week in the
 485 absence of light (– hv) and under a 500 W lamp (+ hv), each diluted (1:5) in pH 12 D₂O or in
 486 DMSO-*d*₆.
 487

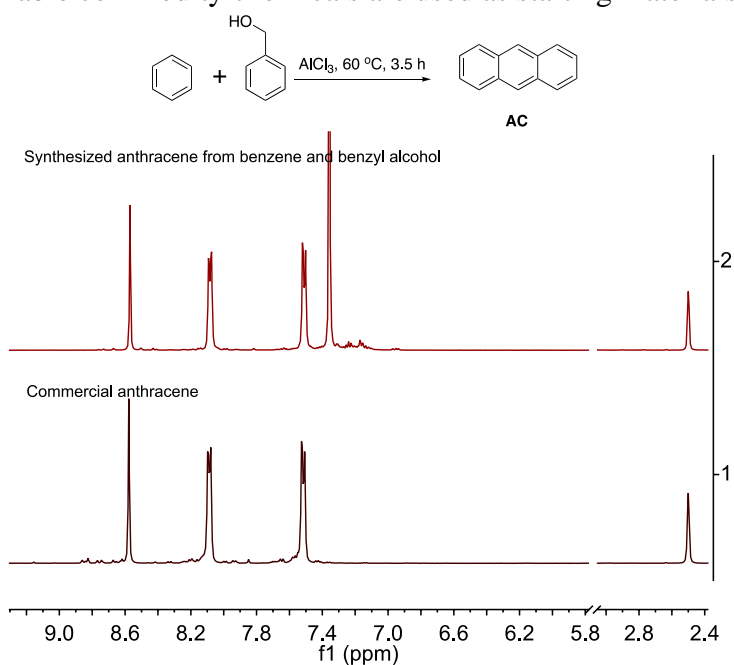
488
489
490

Complete synthesis



491
492
493

Scheme S3. Complete synthetic routes, conditions, and yields of DPivOHAQ and DBAQ when commercially available commodity chemicals are used as starting materials.



494
495
496
497
498
499
500
501

Figure S16. ¹H NMR spectra of commercial and synthesized anthracene (AC) in DMSO-*d*₆. The peak at 7.37 ppm in the synthesized AC spectrum is from benzene.

REFERENCES

- S1 H.-J. Schäfer, *Topics in Current Chemistry*, 1990, **152**, 91–151.
S2. M. Wu, Y. Jing, A. A. Wong, E. M. Fell, S. Jin, Z. Tang, R. G. Gordon and M. J. Aziz, *Chem*, 2020, **6**, 1432–1442.

- 502 S3. G. Maier, L. H. Franz, H.-G. Hartan, K. Lanz and H. P. Reisenauer, *Chemische Berichte*, 1985,
503 **118**, 3196–3204.
- 504 S4. B. E. Hulme, E. J. Land and G. O. Phillips, *J. Chem. Soc. Faraday Trans. 1*, 1972, **68**, 1992–2002.
- 505 S5. S. A. Carlson and D. M. Hercules, *Analytical Chemistry*, 1973, **45**, 1794–1799.
- 506 S6. D. M. Hercules, S. A. Carlson, *Analytical Chemistry* 1974, **46**, 674–678.
- 507 S7. A. D. Broadbent, R. P. Newton, *Canadian Journal of Chemistry* 1972, **50**, 381–387.

508